

LIGHT-X: GENERATIVE 4D VIDEO RENDERING WITH CAMERA AND ILLUMINATION CONTROL

Tianqi Liu^{1,2,3}, Zhaoxi Chen¹, Zihao Huang^{1,2,3}, Shaocong Xu², Saining Zhang^{2,4},
Chongjie Ye⁵, Bohan Li^{6,7}, Zhiguo Cao³, Wei Li¹, Hao Zhao^{4,2†}, Ziwei Liu^{1†}

¹S-Lab, NTU ²BAAI ³HUST ⁴AIR,THU ⁵FNii, CUHKSZ ⁶SJTU ⁷EIT (Ningbo)

<https://lightx-ai.github.io/>

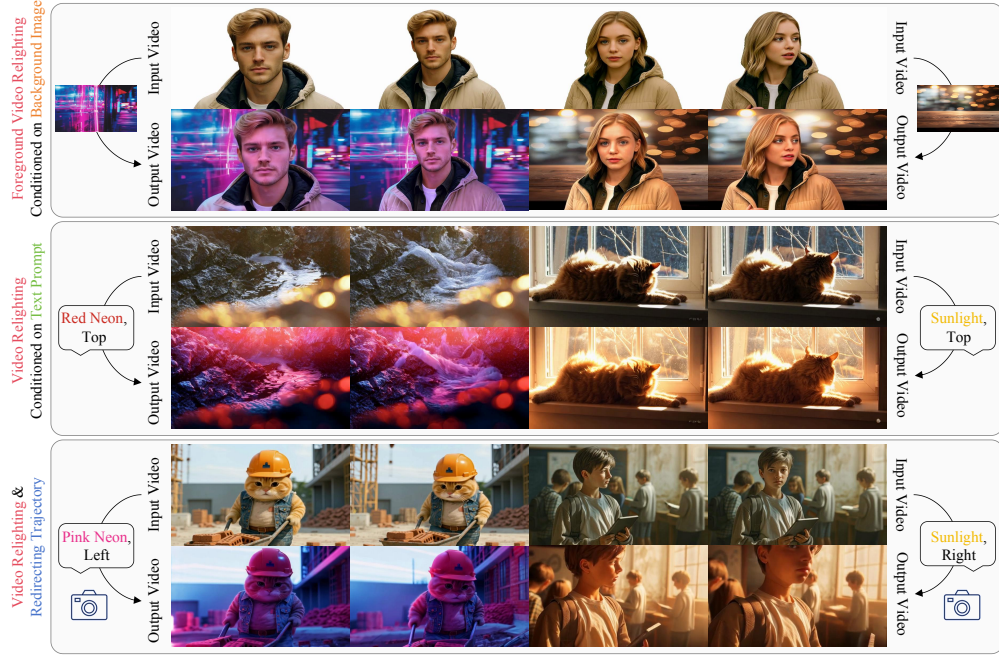


Figure 1: **Light-X** enables controllable video relighting and redirection from monocular video inputs, supporting illumination editing guided by either background images (**top**) or text prompts (**middle**), as well as camera trajectory redirection with user-defined trajectories (**bottom**).

ABSTRACT

Recent advances in illumination control extend image-based methods to video, yet still facing a trade-off between lighting fidelity and temporal consistency. Moving beyond relighting, a key step toward generative modeling of real-world scenes is the joint control of camera trajectory and illumination, since visual dynamics are inherently shaped by both geometry and lighting. To this end, we present **Light-X**, a video generation framework that enables controllable rendering from monocular videos with both viewpoint and illumination control. **1)** We propose a disentangled design that decouples geometry and lighting signals: geometry and motion are captured via dynamic point clouds projected along user-defined camera trajectories, while illumination cues are provided by a relit frame consistently projected into the same geometry. These explicit, fine-grained cues enable effective disentanglement and guide high-quality illumination. **2)** To address the lack of paired multi-view and multi-illumination videos, we introduce **Light-Syn**, a degradation-based pipeline with inverse-mapping that synthesizes training pairs from in-the-wild monocular footage. This strategy yields a dataset covering static, dynamic, and AI-generated scenes, ensuring robust training. Extensive experiments show that Light-X outperforms baseline methods in joint camera-illumination control and surpasses prior video relighting methods under both text- and background-conditioned settings.

† Corresponding authors.

1 INTRODUCTION

Real-world scenes are inherently rich, dynamic, and high-dimensional, shaped jointly by geometry, motion, and illumination. Yet monocular videos, the dominant medium for capturing everyday life, record only a 2D projection of this complexity. Unlocking controllable video generation with camera and illumination control would allow us to revisit such footage from novel viewpoints and under diverse lighting, thereby enabling immersive AR/VR experiences and flexible filmmaking pipelines.

Progress toward this goal has evolved along two largely independent lines of research: video relighting and camera-controlled video generation. **In the relighting domain**, existing video relighting methods typically extend single-image pipelines such as IC-Light (Zhang et al., 2025b) to the video setting, either through training-free fusion (Zhou et al., 2025) or by introducing architectural modifications (Fang et al., 2025). But they suffer from a fundamental trade-off between lighting fidelity and temporal coherence, and crucially, they do not support camera control. **On the other hand**, camera-controlled video generation approaches (YU et al., 2025; Bai et al., 2025; Zhang et al., 2025a; Liu et al., 2025a) enable novel-view video synthesis with accurate camera motion and strong spatio-temporal consistency. However, they are limited to viewpoint manipulation and lack the ability to edit illumination, leaving the joint control of lighting and camera trajectory an open challenge.

In this paper, we aim to develop a video generation model that jointly controls camera trajectory and illumination from monocular videos. This goal raises two key challenges: **1) Joint control.** Controlling camera trajectory and illumination together is inherently difficult, as it demands disentangled yet coherent modeling of geometry, motion, and lighting. Even for video relighting alone, existing methods struggle to balance lighting fidelity with temporal consistency. Viewpoint changes exacerbate this trade-off, making joint camera–illumination control especially challenging. **2) Data scarcity.** Training requires paired multi-view and multi-illumination videos to disentangle geometry and lighting, but such data are unavailable in real-world settings.

To address these challenges, we propose the following solutions. **1) Disentangled control formulation.** We introduce a conditioning scheme that explicitly decouples geometry/motion from illumination. Camera trajectories are modeled through dynamic point cloud rendering like (YU et al., 2025), while illumination cues are provided by projecting a relit frame (obtained via (Zhang et al., 2025b)) into the same geometry, so that the model simultaneously receives projected original frames for geometry and motion, and a projected relit frame for lighting. These fine-grained cues greatly facilitate model learning. In addition, we introduce a light-DiT layer that enforces global illumination consistency. **2) Degradation-based data curation.** Since paired multi-view and multi-illumination videos are scarce, we design Light-Syn, a degradation-based pipeline with inverse mapping that synthesizes training pairs from in-the-wild footage. Degraded video variants (*e.g.*, relit or edited) serve as inputs, while the originals provide supervision¹. By applying the inverse mapping of the degradation process, we project geometry and lighting cues from the original video into the degraded view, yielding diverse pairs from AI-generated, static, and dynamic scenes for robust generalization.

Building on these foundations, we present Light-X, the first framework for video generation with joint control of camera and illumination from monocular videos. As shown in Fig. 1, by decoupling camera and lighting conditioning, our method supports joint camera–illumination control, video relighting, and novel-view synthesis within a single model. Extensive evaluations demonstrate that our approach consistently outperforms baselines in joint camera–illumination control (Table 1). For individual tasks, it delivers superior lighting fidelity and temporal consistency in video relighting under both text (Table 3) and background conditions (Table 5). In addition, a soft-weighted illumination mask enables seamless integration of diverse lighting cues, such as environment maps and reference images, further improving the flexibility.

In summary, **1)** We propose Light-X, the first framework for video generation with joint control of camera trajectory and illumination from monocular videos. **2)** We develop Light-Syn, a degradation-based data pipeline with inverse geometric mapping, which constructs paired training data under controlled camera viewpoints and lighting. **3)** We introduce a disentangled conditioning scheme that explicitly separates geometry and motion from illumination cues, enabling both independent and coupled control. **4)** Extensive experiments show that Light-X achieves SOTA performance in joint camera–illumination control and video relighting under text- and background-conditioned settings.

¹As method outputs are typically lower in fidelity than natural footage, we refer to them as *degraded*.

2 RELATED WORK

Video Generative Models have progressed from GANs (Goodfellow et al., 2020; Clark et al., 2019; Tulyakov et al., 2018; Vondrick et al., 2016; Wang et al., 2020) and VAEs (Kingma & Welling, 2013; Kalchbrenner et al., 2017; Mathieu et al., 2015; Ranzato et al., 2014; Wu et al., 2021) to autoregressive transformers (Wu et al., 2022). Then research focuses shifted to diffusion models (Ho et al., 2020). VDM (Ho et al., 2022) first used a 3D U-Net for video synthesis, and Make-A-Video (Singer et al., 2023) improved resolution and frame rate via super-resolution and interpolation. Latent diffusion (Rombach et al., 2022) was later adopted for efficiency (Blattmann et al., 2023; Zhou et al., 2022; He et al., 2022; Xing et al., 2023; Chen et al., 2024b; Guo et al., 2023b; Wang et al., 2024b). Most recently, Sora (Brooks et al., 2024) demonstrated the scalability of Diffusion Transformers (DiT) (Peebles & Xie, 2023), inspiring many DiT-based models (Wan et al., 2025; Yang et al., 2024b; Kong et al., 2024; Fan et al., 2025; Ma et al., 2025; Lin et al., 2024). Building on these advances, we leverage video diffusion priors for controllable video synthesis.

Learning-Based Illumination Control enables manipulation of scene lighting in images or videos. Early studies leveraged physical illumination models (Barron & Malik, 2014) or deep networks with explicit lighting representations (Zhou et al., 2019; Sun et al., 2019), especially for portraits (Shu et al., 2017; Shih et al., 2014; Sengupta et al., 2018; Chen & Liu, 2022). The recent success of diffusion models has greatly advanced relighting fidelity (Cha et al., 2025; Jin et al., 2024; Kim et al., 2024; Zhang et al., 2025b; He et al., 2025; Liang et al., 2025; Chaturvedi et al., 2025; Chadebec et al., 2025). IC-Light (Zhang et al., 2025b) employs a light-transport consistency loss with large-scale datasets to achieve high-quality image relighting. Recent works (Zhou et al., 2025; Fang et al., 2025; Zeng et al., 2025; Lin et al., 2025) have extended image relighting to videos. Light-A-Video (Zhou et al., 2025) employs cross-frame light attention and progressive fusion in a training-free manner, while RelightVid (Fang et al., 2025) extends IC-Light’s 2D U-Net to a 3D backbone with temporal attention. Yet, these methods still struggle with the trade-off between lighting fidelity and temporal consistency. In this paper, we propose a unified video generation framework that achieves temporally consistent and high-fidelity video relighting, while also supporting camera control.

Camera-Controlled Video Generation. Recent advances in video generation have emphasized conditional signals for controllable synthesis (Yin et al., 2023; Guo et al., 2023a; Xing et al., 2024; Fu et al., 2024). Camera-controlled methods (Yang et al., 2024a; Bahmani et al., 2024; Zheng et al., 2024; 2025) integrate camera parameters into diffusion models for viewpoint control. In static scenes, pose-conditioned diffusion has evolved from object-level (Liu et al., 2023c;d; Long et al., 2023; Tang et al., 2024; Chen et al., 2025b; Ye et al., 2025) to scene-level methods (Gao et al., 2024; Ren et al., 2025; Sargent et al., 2023; Liu et al., 2024; Yu et al., 2024). For dynamic settings, some methods (Wang et al., 2024c; He et al., 2024; Sun et al., 2024; Xiao et al., 2024; Bai et al., 2025; Li et al., 2025a) exploit camera parameters or trajectories for novel-view videos, while others (Wu et al., 2025; Kuang et al., 2024; Bian et al., 2025; Liu et al., 2025a; Wang et al., 2025a) develop multi-view video diffusion. Another direction (You et al., 2025; Gu et al., 2025; Zhang et al., 2025a; YU et al., 2025) leverages explicit geometric cues such as depth or tracking to guide camera control. However, existing methods remain focused solely on camera trajectory control. We instead pursue joint control of camera motion and illumination for high-quality, controllable video generation.

3 METHOD

Given a monocular source video $\mathbf{V}^s = \{\mathbf{I}_i^s\}_{i=1}^f$, our objective is to synthesize a target video $\mathbf{V}^t = \{\mathbf{I}_i^t\}_{i=1}^f$ of the same dynamic scene, but re-rendered under user-specified camera trajectories and illumination conditions. The camera trajectory is denoted as $\mathcal{C} := \{[\mathbf{R}_i, \mathbf{t}_i] \in \mathbb{R}^{3 \times 4}\}_{i=1}^f$, where \mathbf{R}_i and \mathbf{t}_i represent the rotation and translation of the i -th frame relative to the original coordinate system. The illumination condition is denoted as \mathcal{L} , which may be provided in various forms (*e.g.*, a text prompt, an HDR environment map, or a reference image) and will be discussed later. The generated video \mathbf{V}^t should faithfully preserve the appearance and dynamics of \mathbf{V}^s while adhering to \mathcal{C} and \mathcal{L} . In the following sections, we first introduce the camera–illumination decoupling strategy (Sec. 3.1), then present the camera–illumination conditioned video diffusion model (Sec. 3.2). We next describe the data curation pipeline Light-Syn (Sec. 3.3) and finally discuss the framework’s flexibility under diverse illumination conditions (Sec. 3.4).

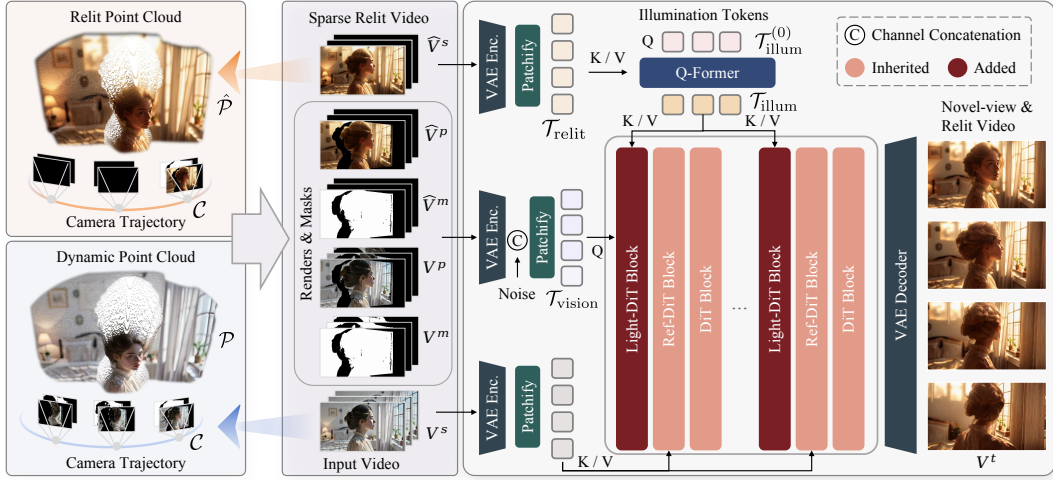


Figure 2: Overview of **Light-X**. Given an input video V^s , we first relight one frame with (Zhang et al., 2025b), conditioned on a lighting text prompt, to obtain a sparse relit video \hat{V}^s . We then estimate depths to construct a dynamic point cloud \mathcal{P} from V^s and a relit point cloud $\hat{\mathcal{P}}$ from \hat{V}^s . Both point clouds are projected along a user-specified camera trajectory, producing geometry-aligned renders and masks (V^p, V^m) and (\hat{V}^p, \hat{V}^m) . These six cues, together with illumination tokens extracted via a Q-Former, are fed into DiT blocks for conditional denoising. Finally, a VAE decoder reconstructs a high-fidelity video V^t faithful to the target trajectory and illumination.

3.1 FORMULATION: CAMERA-ILLUMINATION DECOUPLING

As illustrated in Fig. 2, given a input source video V^s , we disentangle camera and illumination control by constructing two point clouds that separately encode geometric and lighting information.

Camera control. To accurately regulate the camera trajectory, inspired by (Yu et al., 2024; YU et al., 2025; Guo et al., 2025; Hu et al., 2025), we leverage dynamic point clouds as an explicit inductive bias for modeling viewpoint transformations. Concretely, we first estimate a sequence of depth maps $D^s = \{D_i^s\}_{i=1}^f$ from the source video V^s using video depth estimation approaches (Hu et al., 2024). Each frame is then back-projected to 3D space to form a dynamic point cloud $\mathcal{P} = \{P_i\}_{i=1}^f$:

$$P_i = \Phi^{-1}(I_i^s, D_i^s; K), \quad (1)$$

where Φ^{-1} denotes the inverse perspective projection and $K \in \mathbb{R}^{3 \times 3}$ is the camera intrinsics matrix. Given a user-specified trajectory $\mathcal{C} = \{[R_i, t_i]\}_{i=1}^f$, the point clouds are projected into the target viewpoints, yielding geometry-aligned views $V^p = \{I_i^p\}_{i=1}^f$ and visibility masks $V^m = \{M_i^p\}_{i=1}^f$:

$$I_i^p, M_i^p = \Phi(R_i P_i + t_i; K). \quad (2)$$

Together, these projected views and their masks serve as a strong geometric prior, guiding the diffusion model to produce videos that remain geometrically coherent along the specified trajectory.

Illumination control. For illumination, we apply IC-Light (Zhang et al., 2025b) to an arbitrary frame from the source video (the first frame is used for illustration in Fig. 2), producing an image relit according to the desired textual prompt. Subsequently, we construct a sparse relit video $\hat{V}^s = \{\hat{I}_i^s\}_{i=1}^f$, in which the relit frame is retained while all other frames remain blank. Using the previously estimated depths $\{D_i^s\}$, together with the camera intrinsics K and extrinsics $\{[R_i, t_i]\}$, this sparse relit video is lifted into a relit point cloud $\hat{\mathcal{P}} = \{\hat{P}_i\}_{i=1}^f$:

$$\hat{P}_i = \Phi^{-1}(\hat{I}_i^s, D_i^s; K). \quad (3)$$

We reuse the depths predicted from the original video, rather than estimating them again from the relit video, to ensure geometric alignment between the relit and original content. Analogous to the source video branch, the relit point cloud is projected along the target trajectory, yielding geometrically

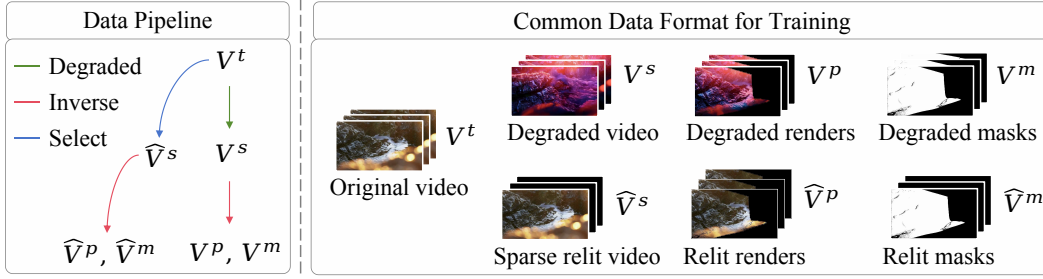


Figure 3: Overview of **Light-Syn**. From an in-the-wild video V^t , we generate a degraded V^s and derive renders, masks (V^p, V^m), and relit counterparts (\hat{V}^p, \hat{V}^m) via inverse transformations.

aligned relit views $\hat{V}^p = \{\hat{I}_i^p\}_{i=1}^f$ with corresponding binary masks $\hat{V}^m = \{\hat{M}_i^p\}_{i=1}^f$, which indicate where illumination information is available and serve as lighting cues:

$$\hat{I}_i^p, \hat{M}_i^p = \Phi(\mathbf{R}_i \hat{\mathbf{P}}_i + \mathbf{t}_i; \mathbf{K}). \quad (4)$$

3.2 ARCHITECTURE: CAMERA-ILLUMINATION CONDITIONED VIDEO DIFFUSION

With the obtained projected source views V^p and masks V^m , together with the relit projections \hat{V}^p and masks \hat{V}^m , the target video can be formulated as a conditional distribution as

$$\mathbf{x} \sim p(\mathbf{x} \mid \mathbf{V}^s, \hat{\mathbf{V}}^s, \mathbf{V}^p, \hat{\mathbf{V}}^p, \mathbf{V}^m, \hat{\mathbf{V}}^m), \quad (5)$$

which not only provides explicit geometric and illumination cues, but also disentangles the two factors in a geometrically aligned space, offering fine-grained guidance and enabling effective learning.

Fine-grained cues. The conditional cues V^p, V^m, \hat{V}^p , and \hat{V}^m are first fed into the VAE encoder. The resulting latents are concatenated with sampled noise (see the middle of Fig. 2) along the channel dimension and then patchified into a sequence of vision tokens $\mathcal{T}_{\text{vision}}$. These tokens encode two complementary fine-grained cues: the projected views V^p , which carry scene content, geometry, and motion, and the projected relit views \hat{V}^p , which provide illumination cues. These tokens are then merged along the sequence axis with text tokens $\mathcal{T}_{\text{text}}$ (not shown in Fig. 2 due to space limit) obtained from the source video via (Li et al., 2022) and (Raffel et al., 2020). The fused text-vision tokens are then passed through DiT blocks for denoising.

Global control. While the rendered fine-grained cues facilitate learning of camera and illumination control, we observe that illumination strength gradually diminishes as the synthesized frames move further away from the relit frame. To mitigate this issue, we introduce a global illumination control module. Specifically, we encode the relit frame with a VAE encoder and patchify its latent to obtain the relit token $\mathcal{T}_{\text{relit}}$. Inspired by (Liu et al., 2023a; Xing et al., 2023), we employ a Q-Former (Li et al., 2023) to extract illumination information. A set of learnable illumination tokens $\mathcal{T}_{\text{illum}}^{(0)}$ serves as queries, while the relit token $\mathcal{T}_{\text{relit}}$ provides the keys and values (Fig. 2 right top). The resulting tokens $\mathcal{T}_{\text{illum}}$ are then injected into our introduced Light-DiT layer through cross-attention:

$$\mathcal{T}_{\text{vision}}' = \text{CrossAttn}(Q = \mathcal{T}_{\text{vision}}, K = V = \mathcal{T}_{\text{illum}}) \quad (6)$$

In addition, we retain the original DiT and Ref-DiT modules from (YU et al., 2025), which respectively aggregate text-vision information and preserve 4D consistency with the input source video.

3.3 DATA CURATION

Effective training requires paired videos with varied camera viewpoints and illumination, yet collecting such data in the real world is almost infeasible. We first analyze the training data requirements in detail and then introduce Light-Syn, a degradation-based pipeline with inverse mapping for synthesizing paired data from in-the-wild monocular videos, as illustrated in Fig. 3.

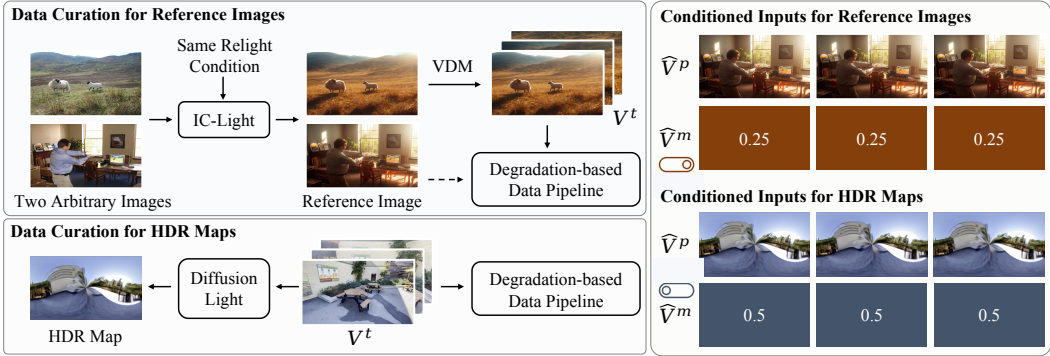


Figure 4: Left: Data curation pipelines for reference-image and HDR-map conditioned video generation. Right: Conditioning cues with soft masks used for model training.

Training Data Requirements. Our model takes as input a source video V^s , a target video V^t , and conditioning sequences V^p , \hat{V}^s , and \hat{V}^p , each with specific requirements. The target V^t should have high quality and consistency, and the input V^s must remain 4D-consistent with V^t in overlapping regions. Projected source views V^p provide reliable geometric priors aligned with the target, while the sparse relit video \hat{V}^s provides explicit illumination cues matching the target’s lighting, and the projected relit views \hat{V}^p deliver fine-grained lighting information geometrically aligned with V^p .

Light-Syn Pipeline. To construct such training pairs, we take an in-the-wild video as target V^t , degrade it to obtain V^s , and record the degradation transformations. Applying their inverses transfers the geometry and illumination of V^t onto V^s , producing spatially aligned conditioning cues. We curate our dataset from three complementary sources: static scenes (8k), dynamic scenes (8k), and AI-generated videos (2k), where the first provide accurate multi-view data, the second capture realistic motion, and the third enrich illumination diversity. All sources satisfy the training requirements, yielding paired inputs, targets, and geometrically aligned conditioning cues. Detailed construction procedures are illustrated in Fig. C and described in detail in Sec. B of the Appendix.

3.4 FRAMEWORK FLEXIBILITY

Camera–illumination decoupled control. Although our training data are curated for joint control, the decoupling and masking mechanisms also allow for independent usage flexibly. For camera control, the conditioned relit frame is replaced with the original frame to preserve lighting. For illumination control (*i.e.*, video relighting), we set $V^p = V^s$, make V^m fully visible, and substitute \hat{V}^p with the sparse relit video \hat{V}^s , with \hat{V}^m updated accordingly. Our framework also supports foreground video relighting conditioned on background images, where V^s is composed of the foreground video and background using foreground masks, and the sparse relit video \hat{V}^s is generated with IC-Light (Zhang et al., 2025b). Further details are provided in Sec. A.2 of the Appendix.

Extension to diverse illumination conditions. Our framework has the potential to accommodate diverse illumination hints as conditioning inputs, such as HDR environment maps and reference images. A reference image here denotes an image from a different scene that conveys lighting information, analogous to a style-transfer source. As shown in Fig. 4, we extend the data curation pipeline accordingly. For HDR maps, we extract environment lighting with DiffusionLight (Phongthawee et al., 2024) and apply the degradation pipeline to obtain 16k samples from (Wang et al., 2023; Ling et al., 2024). For reference-image conditioning, we generate pairs of IC-Light (Zhang et al., 2025b) relit images with matched prompts (Lin et al., 2014; Team, 2024): one serves as the illumination reference, while the other is animated into V^t by a commercial video model (Team, 2024), yielding about 1k samples for each of the text- and background-conditioned settings. During training, conditioning inputs are assigned by modality:

$$(\hat{V}^p, \hat{V}^m) = (V_k, \alpha_k \mathbf{1}), \quad k \in \{\text{ref}, \text{hdr}\}, \quad (7)$$

with $\alpha_{\text{ref}} = 0.25$ and $\alpha_{\text{hdr}} = 0.50$. These soft masks act as domain indicators (Chen et al., 2025a), enabling a single model to generalize across diverse illumination conditions.

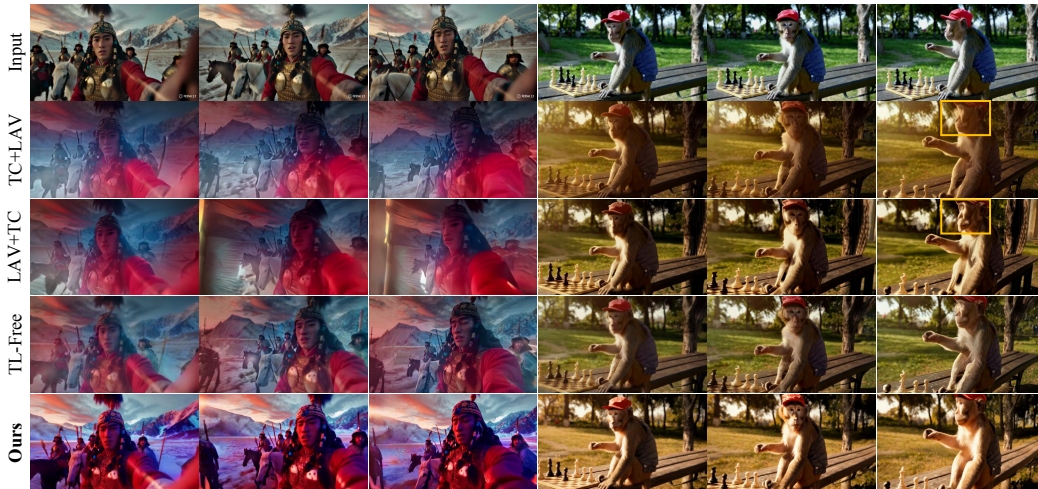


Figure 5: Qualitative comparison for camera-illumination control with light prompts “neon light” (left) and “sunlight” (right). Our method outperforms baselines in relighting quality, temporal consistency, and novel-view content generation. Refer to the supplementary video for clearer comparisons.

Table 1: Quantitative results for the joint camera-illumination control task. User preference indicates the percentage of participants who selected our method.

Method	Image Quality		Video Smoothness		User Study (% , Ours)				Time ↓
	FID ↓	Aesthetic ↑	Motion Pres. ↓	CLIP ↑	RQ	VS	IP	4DC	
TC+IC-Light	/	0.573	6.558	0.976	89.3	91.7	88.3	88.5	3.25 min
TC+LAV	138.89	0.574	4.327	0.986	86.0	84.4	88.0	89.0	4.33 min
LAV+TC	144.61	0.596	5.027	0.987	85.1	89.3	88.8	87.5	4.33 min
TL-Free	122.73	0.595	3.356	0.987	88.0	89.2	88.2	88.2	5.50 min
Ours	101.06	0.623	2.007	0.989	/	/	/	/	1.83 min

4 EXPERIMENTS

4.1 EXPERIMENTAL SETTINGS

Baselines. Our evaluation focuses on two tasks: joint camera-illumination control and video relighting. For the joint control, as no prior work addresses it directly, we construct baselines by combining existing methods: TrajectoryCrafter (TC) (YU et al., 2025)+IC-Light (Zhang et al., 2025b), Light-A-Video (LAV) (Zhou et al., 2025)+TC, TC+LAV, and a training-free baseline TL-Free (Sec. A.1). For video relighting, we assess both text- and background-conditioned settings, comparing with IC-Light (Zhang et al., 2025b), IC-Light+AnyV2V (Ku et al., 2024), Light-A-Video (Zhou et al., 2025), and RelightVid (Fang et al., 2025). We use the Wan2.1 (Wan et al., 2025) implementation of LAV with default hyperparameters. As RelightVid currently offers only a background-conditioned model, we evaluate it exclusively in that setting. More details are provided in Sec. A.3 of the Appendix.

Metrics. Following (Zhou et al., 2025), the evaluation focuses on two aspects: relighting quality and temporal consistency. Relighting quality is measured by FID (Heusel et al., 2017) between each method’s outputs and frame-wise IC-Light results, and by the Aesthetic Preference metric, defined as the mean of the aesthetic score and image quality in (Huang et al., 2024). Temporal consistency is assessed through the average CLIP (Radford et al., 2021) similarity between consecutive frames and Motion Preservation, computed as the deviation between RAFT (Teed & Deng, 2020) estimated optical flow and that of the source video. Considering that IC-Light-referenced FID may induce a bias toward the reference model, we additionally perform an evaluation that compares model outputs directly against real in-the-wild videos. In this evaluation protocol, real videos are treated as ground truth. Their lighting descriptions are extracted using LLaVA (Liu et al., 2023b), and a degraded counterpart is synthesized using LAV (Zhou et al., 2025) under a neutral-lighting prompt to serve as

Table 2: Evaluation of joint camera–illumination control using real in-the-wild videos as reference.

Method	PSNR \uparrow	SSIM \uparrow	LPIPS \downarrow	FVD \downarrow
TC + IC-Light	10.96	0.456	0.474	58.85
TC + LAV	12.18	0.470	0.508	73.78
LAV + TC	12.48	0.463	0.479	60.95
TL-Free	13.49	0.547	0.418	54.44
Ours	13.96	0.582	0.378	45.91

Table 3: Quantitative results for video relighting. * indicates evaluation on the first 16 frames.

Method	Image Quality		Video Smoothness		User Study (% , Ours)			Time \downarrow
	FID \downarrow	Aesthetic \uparrow	Motion Pres. \downarrow	CLIP \uparrow	RQ	VS	IP	
IC-Light	/	0.632	3.293	0.983	88.3	90.3	91.7	1.42 min
LAV	112.45	0.614	2.115	0.991	85.2	88.5	92.5	2.50 min
Ours	83.65	0.645	1.137	0.993	/	/	/	1.50 min
IC-Light+AnyV2V	106.05	0.612	3.777	0.985	97.6	95.1	98.4	1.67 min
Ours*	77.97	0.625	1.452	0.992	/	/	/	/

the model input. At test time, the degraded video is paired with its LLaVA-inferred lighting prompt, which is provided as the illumination condition. The relit outputs are then assessed against the real videos using standard perceptual and temporal metrics, including PSNR, SSIM (Wang et al., 2004), LPIPS (Zhang et al., 2018), and FVD (Unterthiner et al., 2019). We also conduct a user study with 57 participants to evaluate relighting quality (RQ, lighting fidelity and alignment with the prompt), video smoothness (VS), ID preservation (IP, consistency of the object’s identity and albedo after relighting), and 4D consistency (4DC, spatio-temporal coherence in the novel-view setting). During evaluation, lighting prompts, directions, and camera trajectories are randomly sampled for each video.

Datasets. For evaluation data, we collect 200 high-quality videos from sources including Pexels (Pexels, 2025), Sora (Brooks et al., 2024), and Kling (Team, 2024). These videos cover a wide range of subjects such as humans, animals, and objects, across diverse scenes with substantial motion, incorporating both in-the-wild and AI-generated content. For background conditioned relighting, we use 10 background images and 30 foreground videos from (Zhang et al., 2025b) and (Team, 2024), producing 300 combinations. None of these videos is used for training in any compared methods.

Implementation Details. The framework is based on (YU et al., 2025; CogVideoX-Fun, 2024; Yang et al., 2024b). Training uses videos of resolution 384×672 and 49 frames, for 16,000 iterations with a learning rate of 2×10^{-5} and a batch size of 8 on eight H100 GPUs. Video depths are estimated with (Hu et al., 2024) to construct dynamic point clouds, with camera intrinsics set empirically.

4.2 CAMERA-ILLUMINATION CONTROL RESULTS

Qualitative results are shown in Fig. 5 and better inspected in supplementary videos. TC (YU et al., 2025)+LAV (Zhou et al., 2025) is limited by LAV’s weak relighting, especially under large camera motion, causing poor lighting quality and temporal instability. For LAV+TC, relit outputs degrade point cloud reconstruction, leading TC to produce artifacts from novel viewpoints. TL-Free suffers from a trade-off between fidelity and consistency. In contrast, our approach achieves a good balance of relighting quality, novel-view synthesis, and temporal stability, and outperforms all baselines in both fidelity and smoothness, as demonstrated in Table 1. Additional visual results are provided in Fig. Q in the Appendix. We further assess joint camera-illumination control using real in-the-wild videos as ground truth. As reported in Table 2, our method achieves the best PSNR, SSIM, LPIPS, and FVD scores, further confirming its advantages in both lighting fidelity and temporal consistency. User studies further validate these improvements.

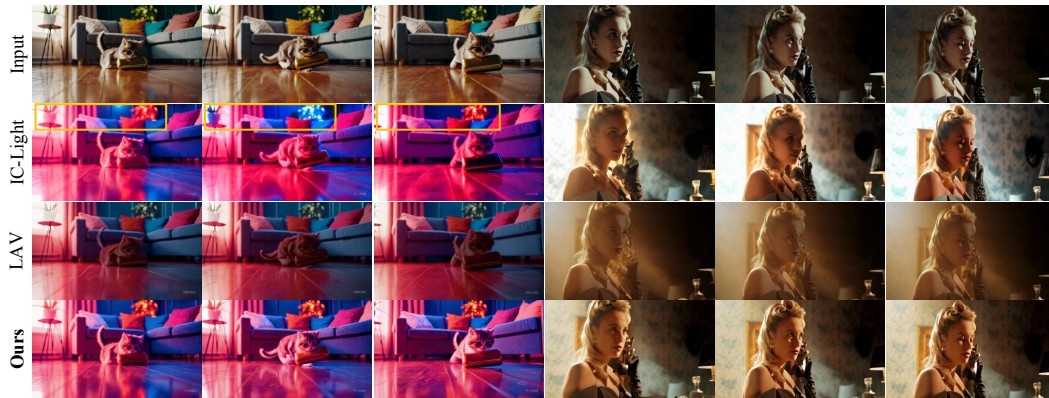


Figure 6: Qualitative comparison for video relighting with light prompts “neon light” (left) and “sunlight” (right). Our method outperforms baseline methods in both relighting quality and temporal consistency. Please refer to the supplementary video for clearer comparisons.

Table 4: Evaluation of video relighting using real in-the-wild videos as reference.

Method	PSNR \uparrow	SSIM \uparrow	LPIPS \downarrow	FVD \downarrow
IC-Light	11.75	0.517	0.422	67.50
LAV	12.66	0.530	0.429	74.64
Ours	13.84	0.581	0.369	56.60

Table 5: Quantitative results for background image-conditioned foreground video relighting. Methods marked with * are evaluated on the first 16 frames.

Method	Image Quality		Video Smoothness		User Study (% , Ours)		
	FID \downarrow	Aesthetic \uparrow	Motion Preservation \downarrow	CLIP \uparrow	RQ	VS	IP
IC-Light	/	0.645	0.374	0.987	81.8	91.7	88.0
Light-A-Video	76.05	0.619	0.296	0.990	85.5	87.1	88.0
Ours	61.75	0.680	0.220	0.992	/	/	/
RelightVid	86.94	0.635	0.230	0.988	81.8	87.1	87.3
Ours*	56.60	0.682	0.199	0.990	/	/	/

4.3 VIDEO RELIGHTING RESULTS

Text-conditioned relighting. Fig. 6 and Fig. R in the Appendix show qualitative comparisons. Frame-wise IC-Light (Zhang et al., 2025b) achieves high single-frame quality but lacks temporal constraints, causing flicker in lighting and appearance. LAV (Zhou et al., 2025) integrates VDM (Wan et al., 2025) priors via a training-free fusion, improving stability but reducing fidelity. Our method attains both significant lighting accuracy and temporal coherence. Quantitative results in Table 3 confirm consistent gains in relighting fidelity and temporal smoothness, further supported by user studies. We additionally evaluate text-conditioned relighting using real in-the-wild videos as ground truth. As shown in Table 4, our method achieves the best performance across all metrics, further demonstrating its strengths in lighting fidelity and temporal stability.

Background-conditioned relighting. We also evaluate foreground video relighting conditioned on background images. As shown in Table 5, our method surpasses all baselines in both image quality and video smoothness. The corresponding qualitative analyses are provided in Sec. D.3. Additionally, we present results for HDR map-conditioned relighting (Sec. D.4) and reference image-conditioned relighting (Sec. D.5) in the Appendix.

Table 6: Qualitative ablation results for the joint camera-illumination control across different components: (a) training data, (b) architecture and lighting conditions, (c) training and conditioning strategy.

Method	FID Score ↓	Aesthetic ↑	Motion Pres. ↓	CLIP Score ↑
(a.i) w/o static data	123.35	0.594	3.749	0.987
(a.ii) w/o dynamic data	108.70	0.621	2.635	0.988
(a.iii) w/o AI-gen data	102.09	0.613	2.498	0.988
(b.i) w/o fine-grained lighting cues	143.02	0.602	2.242	0.989
(b.ii) w/o global lighting control	103.13	0.612	2.348	0.989
(b.iii) light+text concat	137.05	0.596	2.654	0.989
(c.i) algorithm-generated GT	137.83	0.524	4.066	0.986
(c.ii) relit all frames	71.10	0.571	4.238	0.986
(c.iii) w/o soft mask	148.51	0.545	2.879	0.988
Ours	101.06	0.623	2.007	0.989

4.4 ABLATION STUDIES

We conduct ablation studies on (a) training data, (b) architecture and lighting design, and (c) training and conditioning strategy. Quantitative results are in Table 6, and qualitative comparisons are shown in Fig. D of the Appendix. Removing static data (a.i) weakens unseen-view synthesis, as static videos provide natural cross-view pairs. Excluding dynamic data (a.ii) causes motion artifacts, while omitting AI-generated data (a.iii) lowers robustness to rare lighting, such as neon, where brightness may decay. Skipping fine-grained cues (b.i) limits the use of illumination priors from IC-Light (Zhang et al., 2025b), degrading relighting quality. Disabling global control (b.ii) causes fading or abrupt shifts under complex lighting, whereas adding it stabilizes results. Replacing our conditioning with light-text concatenation (b.iii), as in (Fang et al., 2025), also fails to leverage fine-grained lighting priors. Reversing supervision (c.i) by treating algorithm-generated outputs as ground truth harms fidelity, consistency, and novel-view synthesis. Relighting all frames instead of a single frame (c.ii) increases cost and reduces temporal coherence despite better FID. Discarding the soft mask (c.iii) blurs illumination domains and introduces interference, lowering overall performance.

5 CONCLUSION

We introduce Light-X, the first video generation framework that jointly controls camera trajectory and illumination from monocular videos. Our disentangled conditioning design leverages dynamic point clouds along user-defined trajectories to provide geometry and motion cues, while a relit frame is re-projected into the same geometry to provide illumination cues. To enable training, we further propose Light-Syn, a degradation-based data synthesis pipeline that constructs paired videos without requiring multi-view, multi-illumination captures. Extensive experiments show that Light-X consistently surpasses existing baselines in both joint camera-illumination control and video relighting, while flexibly adapting to diverse lighting conditions. We believe this work paves the way toward scalable generative modeling and controllable editing of complex real-world scenes.

Limitations and Future Work. 1) Our method relies on single-image relighting priors (e.g., IC-Light (Zhang et al., 2025b)) to provide fine-grained lighting cues. In some scenes, the lighting quality of these priors may be suboptimal, which can in turn affect the quality of subsequent video generation. 2) The approach depends on point clouds as priors for novel camera viewpoints. When depth estimation is inaccurate, the resulting biased geometry may degrade generation quality, and the framework also struggles with very wide camera motions (e.g., 360°) due to limited 3D cues and the constrained generation length of the video diffusion model. 3) Like other video diffusion approaches, handling fine details (e.g., hands) remains challenging, and the multi-step denoising process is computationally expensive. Future work may explore stronger video generation backbones (e.g., Wan2.2 (Wan et al., 2025)) to enhance video quality, progressive point-cloud expansion to better support large camera ranges, and techniques such as Diffusion Forcing (Chen et al., 2024a) and Self Forcing (Huang et al., 2025) to extend video length.

REFERENCES

- Sherwin Bahmani, Ivan Skorokhodov, Aliaksandr Siarohin, Willi Menapace, Guocheng Qian, Michael Vasilkovsky, Hsin-Ying Lee, Chaoyang Wang, Jiaxu Zou, Andrea Tagliasacchi, et al. Vd3d: Taming large video diffusion transformers for 3d camera control. *arXiv preprint arXiv:2407.12781*, 2024. [3](#)
- Jianhong Bai, Menghan Xia, Xiao Fu, Xintao Wang, Lianrui Mu, Jinwen Cao, Zuozhu Liu, Haoji Hu, Xiang Bai, Pengfei Wan, et al. Recammaster: Camera-controlled generative rendering from a single video. *arXiv preprint arXiv:2503.11647*, 2025. [2](#), [3](#), [26](#)
- Jonathan T Barron and Jitendra Malik. Shape, illumination, and reflectance from shading. *IEEE transactions on pattern analysis and machine intelligence*, 37(8):1670–1687, 2014. [3](#)
- Weikang Bian, Zhaoyang Huang, Xiaoyu Shi, Yijin Li, Fu-Yun Wang, and Hongsheng Li. Gs-dit: Advancing video generation with pseudo 4d gaussian fields through efficient dense 3d point tracking. *arXiv preprint arXiv:2501.02690*, 2025. [3](#)
- Andreas Blattmann, Tim Dockhorn, Sumith Kulal, Daniel Mendelevitch, Maciej Kilian, Dominik Lorenz, Yam Levi, Zion English, Vikram Voleti, Adam Letts, et al. Stable video diffusion: Scaling latent video diffusion models to large datasets. *arXiv preprint arXiv:2311.15127*, 2023. [3](#)
- Tim Brooks, Bill Peebles, Connor Holmes, Will DePue, Yufei Guo, Li Jing, David Schnurr, Joe Taylor, Troy Luhman, Eric Luhman, Clarence Ng, Ricky Wang, and Aditya Ramesh. Video generation models as world simulators. 2024. URL <https://openai.com/research/video-generation-models-as-world-simulators>. [3](#), [8](#), [20](#)
- Junuk Cha, Mengwei Ren, Krishna Kumar Singh, He Zhang, Yannick Hold-Geoffroy, Seunghyun Yoon, HyunJoon Jung, Jae Shin Yoon, and Seungryul Baek. Text2relight: Creative portrait relighting with text guidance. In *Proceedings of the AAAI Conference on Artificial Intelligence*, volume 39, pp. 1980–1988, 2025. [3](#)
- Clément Chadebec, Onur Tasar, Sanjeev Sreetharan, and Benjamin Aubin. Lbm: Latent bridge matching for fast image-to-image translation. *arXiv preprint arXiv:2503.07535*, 2025. [3](#)
- Sumit Chaturvedi, Mengwei Ren, Yannick Hold-Geoffroy, Jingyuan Liu, Julie Dorsey, and Zhixin Shu. Synthlight: Portrait relighting with diffusion model by learning to re-render synthetic faces. In *Proceedings of the Computer Vision and Pattern Recognition Conference*, pp. 369–379, 2025. [3](#)
- Boyuan Chen, Diego Martí Monsó, Yilun Du, Max Simchowitz, Russ Tedrake, and Vincent Sitzmann. Diffusion forcing: Next-token prediction meets full-sequence diffusion. *Advances in Neural Information Processing Systems*, 37:24081–24125, 2024a. [10](#)
- Haoxin Chen, Yong Zhang, Xiaodong Cun, Menghan Xia, Xintao Wang, Chao Weng, and Ying Shan. Videocrafter2: Overcoming data limitations for high-quality video diffusion models, 2024b. [3](#)
- Zhaoxi Chen and Ziwei Liu. Relighting4d: Neural relightable human from videos. In *ECCV*, 2022. [3](#)
- Zhaoxi Chen, Tianqi Liu, Long Zhuo, Jiawei Ren, Zeng Tao, He Zhu, Fangzhou Hong, Liang Pan, and Ziwei Liu. 4dnex: Feed-forward 4d generative modeling made easy. *arXiv preprint arXiv:2508.13154*, 2025a. [6](#)
- Zhaoxi Chen, Jiaxiang Tang, Yuhao Dong, Ziang Cao, Fangzhou Hong, Yushi Lan, Tengfei Wang, Haozhe Xie, Tong Wu, Shunsuke Saito, Liang Pan, Dahua Lin, and Ziwei Liu. 3dtopia-xl: High-quality 3d pbr asset generation via primitive diffusion. In *CVPR*, 2025b. [3](#)
- Aidan Clark, Jeff Donahue, and Karen Simonyan. Adversarial video generation on complex datasets. *arXiv preprint arXiv:1907.06571*, 2019. [3](#)
- CogVideoX-Fun. Cogvideox-fun, 2024. URL <https://github.com/aigc-apps/CogVideoX-Fun>. [8](#)
- Weichen Fan, Chenyang Si, Junhao Song, Zhenyu Yang, Yinan He, Long Zhuo, Ziqi Huang, Ziyue Dong, Jingwen He, Dongwei Pan, et al. Vchitect-2.0: Parallel transformer for scaling up video diffusion models. *arXiv preprint arXiv:2501.08453*, 2025. [3](#)

- Ye Fang, Zeyi Sun, Shangzhan Zhang, Tong Wu, Yinghao Xu, Pan Zhang, Jiaqi Wang, Gordon Wetzstein, and Dahua Lin. Relightvid: Temporal-consistent diffusion model for video relighting. *arXiv preprint arXiv:2501.16330*, 2025. 2, 3, 7, 10, 18, 23
- Xiao Fu, Xian Liu, Xintao Wang, Sida Peng, Menghan Xia, Xiaoyu Shi, Ziyang Yuan, Pengfei Wan, Di Zhang, and Dahua Lin. 3dtrajmaster: Mastering 3d trajectory for multi-entity motion in video generation. *arXiv preprint arXiv:2412.07759*, 2024. 3
- Hang Gao, Ruilong Li, Shubham Tulsiani, Bryan Russell, and Angjoo Kanazawa. Dynamic novel-view synthesis: A reality check. In *NeurIPS*, 2022. 22, 23, 24
- Ruiqi Gao, Aleksander Holynski, Philipp Henzler, Arthur Brussee, Ricardo Martin-Brualla, Pratul Srinivasan, Jonathan T Barron, and Ben Poole. Cat3d: Create anything in 3d with multi-view diffusion models. *arXiv preprint arXiv:2405.10314*, 2024. 3
- Ian Goodfellow, Jean Pouget-Abadie, Mehdi Mirza, Bing Xu, David Warde-Farley, Sherjil Ozair, Aaron Courville, and Yoshua Bengio. Generative adversarial networks. *Communications of the ACM*, 63(11):139–144, 2020. 3
- Zekai Gu, Rui Yan, Jiahao Lu, Peng Li, Zhiyang Dou, Chenyang Si, Zhen Dong, Qifeng Liu, Cheng Lin, Ziwei Liu, et al. Diffusion as shader: 3d-aware video diffusion for versatile video generation control. In *Proceedings of the Special Interest Group on Computer Graphics and Interactive Techniques Conference Conference Papers*, pp. 1–12, 2025. 3
- Jiazhe Guo, Yikang Ding, Xiwu Chen, Shuo Chen, Bohan Li, Yingshuang Zou, Xiaoyang Lyu, Feiyang Tan, Xiaojuan Qi, Zhiheng Li, and Hao Zhao. Dist-4d: Disentangled spatiotemporal diffusion with metric depth for 4d driving scene generation. *arXiv preprint arXiv:2503.15208*, 2025. 4
- Yuwei Guo, Ceyuan Yang, Anyi Rao, Maneesh Agrawala, Dahua Lin, and Bo Dai. Sparsectrl: Adding sparse controls to text-to-video diffusion models. *arXiv preprint arXiv:2311.16933*, 2023a. 3
- Yuwei Guo, Ceyuan Yang, Anyi Rao, Zhengyang Liang, Yaohui Wang, Yu Qiao, Maneesh Agrawala, Dahua Lin, and Bo Dai. Animatediff: Animate your personalized text-to-image diffusion models without specific tuning. *arXiv preprint arXiv:2307.04725*, 2023b. 3
- Hao He, Yinghao Xu, Yuwei Guo, Gordon Wetzstein, Bo Dai, Hongsheng Li, and Ceyuan Yang. Cameractrl: Enabling camera control for text-to-video generation. *arXiv preprint arXiv:2404.02101*, 2024. 3
- Kai He, Ruofan Liang, Jacob Munkberg, Jon Hasselgren, Nandita Vijaykumar, Alexander Keller, Sanja Fidler, Igor Gilitschenski, Zan Gojcic, and Zian Wang. Unirelight: Learning joint decomposition and synthesis for video relighting. *arXiv preprint arXiv:2506.15673*, 2025. 3
- Yingqing He, Tianyu Yang, Yong Zhang, Ying Shan, and Qifeng Chen. Latent video diffusion models for high-fidelity long video generation. *arXiv preprint arXiv:2211.13221*, 2022. 3
- Martin Heusel, Hubert Ramsauer, Thomas Unterthiner, Bernhard Nessler, and Sepp Hochreiter. Gans trained by a two time-scale update rule converge to a local nash equilibrium. *Advances in neural information processing systems*, 30, 2017. 7
- Jonathan Ho, Ajay Jain, and Pieter Abbeel. Denoising diffusion probabilistic models. In *NeurIPS*, pp. 6840–6851, 2020. 3
- Jonathan Ho, Tim Salimans, Alexey Gritsenko, William Chan, Mohammad Norouzi, and David J Fleet. Video diffusion models. In *NeurIPS*, pp. 8633–8646, 2022. 3
- Tao Hu, Haoyang Peng, Xiao Liu, and Yuwen Ma. Ex-4d: Extreme viewpoint 4d video synthesis via depth watertight mesh. *arXiv preprint arXiv:2506.05554*, 2025. 4
- Wenbo Hu, Xiangjun Gao, Xiaoyu Li, Sijie Zhao, Xiaodong Cun, Yong Zhang, Long Quan, and Ying Shan. Depthcrafter: Generating consistent long depth sequences for open-world videos. *arXiv preprint arXiv:2409.02095*, 2024. 4, 8, 28

- Xun Huang, Zhengqi Li, Guande He, Mingyuan Zhou, and Eli Shechtman. Self forcing: Bridging the train-test gap in autoregressive video diffusion. *arXiv preprint arXiv:2506.08009*, 2025. 10
- Ziqi Huang, Yanan He, Jiashuo Yu, Fan Zhang, Chenyang Si, Yuming Jiang, Yuanhan Zhang, Tianxing Wu, Qingyang Jin, Nattapol Chanpaisit, et al. Vbench: Comprehensive benchmark suite for video generative models. In *Proceedings of the IEEE/CVF Conference on Computer Vision and Pattern Recognition*, pp. 21807–21818, 2024. 7, 20, 23
- Haian Jin, Yuan Li, Fujun Luan, Yuanbo Xiangli, Sai Bi, Kai Zhang, Zexiang Xu, Jin Sun, and Noah Snavely. Neural gaffer: Relighting any object via diffusion. *Advances in Neural Information Processing Systems*, 37:141129–141152, 2024. 3
- Nal Kalchbrenner, Aäron Oord, Karen Simonyan, Ivo Danihelka, Oriol Vinyals, Alex Graves, and Koray Kavukcuoglu. Video pixel networks. In *International Conference on Machine Learning*, pp. 1771–1779. PMLR, 2017. 3
- Hoon Kim, Minje Jang, Wonjun Yoon, Jisoo Lee, Donghyun Na, and Sanghyun Woo. Switchlight: Co-design of physics-driven architecture and pre-training framework for human portrait relighting. In *Proceedings of the IEEE/CVF Conference on Computer Vision and Pattern Recognition*, pp. 25096–25106, 2024. 3
- Diederik P Kingma and Max Welling. Auto-encoding variational bayes. *arXiv preprint arXiv:1312.6114*, 2013. 3, 20
- Weijie Kong, Qi Tian, Zijian Zhang, Rox Min, Zuozhuo Dai, Jin Zhou, Jiangfeng Xiong, Xin Li, Bo Wu, Jianwei Zhang, et al. Hunyuanvideo: A systematic framework for large video generative models. *arXiv preprint arXiv:2412.03603*, 2024. 3, 20
- Max Ku, Cong Wei, Weiming Ren, Harry Yang, and Wenhui Chen. Anyv2v: A tuning-free framework for any video-to-video editing tasks. *arXiv preprint arXiv:2403.14468*, 2024. 7, 18
- Zhengfei Kuang, Shengqu Cai, Hao He, Yinghao Xu, Hongsheng Li, Leonidas Guibas, and Gordon Wetzstein. Collaborative video diffusion: Consistent multi-video generation with camera control. In *arXiv*, 2024. 3
- Bohan Li, Zhuang Ma, Dalong Du, Baorui Peng, Zhujin Liang, Zhenqiang Liu, Chao Ma, Yueming Jin, Hao Zhao, Wenjun Zeng, et al. Omninwm: Omniscient driving navigation world models. *arXiv preprint arXiv:2510.18313*, 2025a. 3
- Junnan Li, Dongxu Li, Caiming Xiong, and Steven Hoi. Blip: Bootstrapping language-image pre-training for unified vision-language understanding and generation. In *International conference on machine learning*, 2022. 5
- Junnan Li, Dongxu Li, Silvio Savarese, and Steven Hoi. Blip-2: Bootstrapping language-image pre-training with frozen image encoders and large language models. In *International conference on machine learning*, pp. 19730–19742. PMLR, 2023. 5
- Zhengqi Li, Richard Tucker, Forrester Cole, Qianqian Wang, Linyi Jin, Vickie Ye, Angjoo Kanazawa, Aleksander Holynski, and Noah Snavely. Megasam: Accurate, fast and robust structure and motion from casual dynamic videos. In *Proceedings of the Computer Vision and Pattern Recognition Conference*, pp. 10486–10496, 2025b. 24
- Ruofan Liang, Zan Gojcic, Huan Ling, Jacob Munkberg, Jon Hasselgren, Chih-Hao Lin, Jun Gao, Alexander Keller, Nandita Vijaykumar, Sanja Fidler, et al. Diffusion renderer: Neural inverse and forward rendering with video diffusion models. In *Proceedings of the Computer Vision and Pattern Recognition Conference*, pp. 26069–26080, 2025. 3, 23, 30
- Bin Lin, Yunyang Ge, Xinhua Cheng, Zongjian Li, Bin Zhu, Shaodong Wang, Xianyi He, Yang Ye, Shenghai Yuan, Liuhan Chen, et al. Open-sora plan: Open-source large video generation model. *arXiv preprint arXiv:2412.00131*, 2024. 3, 20
- Tsung-Yi Lin, Michael Maire, Serge Belongie, James Hays, Pietro Perona, Deva Ramanan, Piotr Dollár, and C Lawrence Zitnick. Microsoft coco: Common objects in context. In *European conference on computer vision*, pp. 740–755. Springer, 2014. 6

- Yuanze Lin, Yi-Wen Chen, Yi-Hsuan Tsai, Ronald Clark, and Ming-Hsuan Yang. Illumicraft: Unified geometry and illumination diffusion for controllable video generation. *arXiv preprint arXiv:2506.03150*, 2025. 3
- Lu Ling, Yichen Sheng, Zhi Tu, Wentian Zhao, Cheng Xin, Kun Wan, Lantao Yu, Qianyu Guo, Zixun Yu, Yawen Lu, et al. D13dv-10k: A large-scale scene dataset for deep learning-based 3d vision. In *Proceedings of the IEEE/CVF Conference on Computer Vision and Pattern Recognition*, pp. 22160–22169, 2024. 6, 19
- Fangfu Liu, Wenqiang Sun, Hanyang Wang, Yikai Wang, Haowen Sun, Junliang Ye, Jun Zhang, and Yueqi Duan. Reconx: Reconstruct any scene from sparse views with video diffusion model. *arXiv preprint arXiv:2408.16767*, 2024. 3
- Gongye Liu, Menghan Xia, Yong Zhang, Haoxin Chen, Jinbo Xing, Xintao Wang, Yujiu Yang, and Ying Shan. Stylecrafter: Enhancing stylized text-to-video generation with style adapter. *arXiv preprint arXiv:2312.00330*, 2023a. 5
- Haotian Liu, Chunyuan Li, Qingyang Wu, and Yong Jae Lee. Visual instruction tuning, 2023b. 7
- Ruoshi Liu, Rundi Wu, Basile Van Hoorick, Pavel Tokmakov, Sergey Zakharov, and Carl Vondrick. Zero-1-to-3: Zero-shot one image to 3d object, 2023c. 3
- Tianqi Liu, Zihao Huang, Zhaoxi Chen, Guangcong Wang, Shoukang Hu, Liao Shen, Huiqiang Sun, Zhiguo Cao, Wei Li, and Ziwei Liu. Free4d: Tuning-free 4d scene generation with spatial-temporal consistency. In *Proceedings of the IEEE/CVF International Conference on Computer Vision (ICCV)*, pp. 25571–25582, October 2025a. 2, 3, 25, 26, 28
- Yang Liu, Chuanchen Luo, Zimo Tang, Yingyan Li, Yuanyong Ning, Lue Fan, Junran Peng, Zhaoxiang Zhang, et al. Tc-light: Temporally coherent generative rendering for realistic world transfer. In *The Thirty-ninth Annual Conference on Neural Information Processing Systems*, 2025b. 26
- Yuan Liu, Cheng Lin, Zijiao Zeng, Xiaoxiao Long, Lingjie Liu, Taku Komura, and Wenping Wang. Syncdreamer: Generating multiview-consistent images from a single-view image. *arXiv preprint arXiv:2309.03453*, 2023d. 3
- Xiaoxiao Long, Yuan-Chen Guo, Cheng Lin, Yuan Liu, Zhiyang Dou, Lingjie Liu, Yuexin Ma, Song-Hai Zhang, Marc Habermann, Christian Theobalt, et al. Wonder3d: Single image to 3d using cross-domain diffusion. *arXiv preprint arXiv:2310.15008*, 2023. 3
- Xin Ma, Yaohui Wang, Xinyuan Chen, Gengyun Jia, Ziwei Liu, Yuan-Fang Li, Cunjian Chen, and Yu Qiao. Latte: Latent diffusion transformer for video generation. *Transactions on Machine Learning Research*, 2025. 3
- Michael Mathieu, Camille Couprie, and Yann LeCun. Deep multi-scale video prediction beyond mean square error. *arXiv preprint arXiv:1511.05440*, 2015. 3
- Kepan Nan, Rui Xie, Penghao Zhou, Tiehan Fan, Zhenheng Yang, Zhijie Chen, Xiang Li, Jian Yang, and Ying Tai. Openvid-1m: A large-scale high-quality dataset for text-to-video generation. *arXiv preprint arXiv:2407.02371*, 2024. 20
- William Peebles and Saining Xie. Scalable diffusion models with transformers. In *ICCV*, 2023. 3, 20
- Pexels. Pexels. <https://www.pexels.com>, 2025. 8
- Pakkapon Phongthawee, Worameth Chinchuthakun, Nontaphat Sinsunthithet, Varun Jampani, Amit Raj, Pramook Khungurn, and Supasorn Suwajanakorn. Diffusionlight: Light probes for free by painting a chrome ball. In *Proceedings of the IEEE/CVF conference on computer vision and pattern recognition*, pp. 98–108, 2024. 6, 23
- Alec Radford, Jong Wook Kim, Chris Hallacy, Aditya Ramesh, Gabriel Goh, Sandhini Agarwal, Girish Sastry, Amanda Askell, Pamela Mishkin, Jack Clark, et al. Learning transferable visual models from natural language supervision. In *International conference on machine learning*, pp. 8748–8763. PmLR, 2021. 7

- Colin Raffel, Noam Shazeer, Adam Roberts, Katherine Lee, Sharan Narang, Michael Matena, Yanqi Zhou, Wei Li, and Peter J. Liu. Exploring the limits of transfer learning with a unified text-to-text transformer. *Journal of Machine Learning Research*, 2020. 5
- MarcAurelio Ranzato, Arthur Szlam, Joan Bruna, Michael Mathieu, Ronan Collobert, and Sumit Chopra. Video (language) modeling: a baseline for generative models of natural videos. *arXiv preprint arXiv:1412.6604*, 2014. 3
- Xuanchi Ren, Tianchang Shen, Jiahui Huang, Huan Ling, Yifan Lu, Merlin Nimier-David, Thomas Müller, Alexander Keller, Sanja Fidler, and Jun Gao. Gen3c: 3d-informed world-consistent video generation with precise camera control. In *Proceedings of the Computer Vision and Pattern Recognition Conference*, pp. 6121–6132, 2025. 3
- Robin Rombach, Andreas Blattmann, Dominik Lorenz, Patrick Esser, and Björn Ommer. High-resolution image synthesis with latent diffusion models. In *CVPR*, 2022. 3, 20
- Kyle Sargent, Zizhang Li, Tanmay Shah, Charles Herrmann, Hong-Xing Yu, Yunzhi Zhang, Eric Ryan Chan, Dmitry Lagun, Li Fei-Fei, Deqing Sun, et al. Zeronvs: Zero-shot 360-degree view synthesis from a single real image. 2023. 3
- Soumyadip Sengupta, Angjoo Kanazawa, Carlos D Castillo, and David W Jacobs. Sfsnet: Learning shape, reflectance and illuminance of faces in the wild. In *Proceedings of the IEEE conference on computer vision and pattern recognition*, pp. 6296–6305, 2018. 3
- YiChang Shih, Sylvain Paris, Connelly Barnes, William T Freeman, and Frédo Durand. Style transfer for headshot portraits. 2014. 3
- Zhixin Shu, Sunil Hadap, Eli Shechtman, Kalyan Sunkavalli, Sylvain Paris, and Dimitris Samaras. Portrait lighting transfer using a mass transport approach. *ACM Transactions on Graphics (TOG)*, 36(4):1, 2017. 3
- Uriel Singer, Adam Polyak, Thomas Hayes, Xi Yin, Jie An, Songyang Zhang, Qiyuan Hu, Harry Yang, Oron Ashual, Oran Gafni, et al. Make-a-video: Text-to-video generation without text-video data. In *ICLR*, 2023. 3
- Tiancheng Sun, Jonathan T Barron, Yun-Ta Tsai, Zexiang Xu, Xueming Yu, Graham Fyffe, Christoph Rhemann, Jay Busch, Paul E Debevec, and Ravi Ramamoorthi. Single image portrait relighting. *ACM Trans. Graph.*, 38(4):79–1, 2019. 3
- Wenqiang Sun, Shuo Chen, Fangfu Liu, Zilong Chen, Yueqi Duan, Jun Zhang, and Yikai Wang. Dimensionx: Create any 3d and 4d scenes from a single image with controllable video diffusion. *arXiv preprint arXiv:2411.04928*, 2024. 3
- Jiaxiang Tang, Zhaoxi Chen, Xiaokang Chen, Tengfei Wang, Gang Zeng, and Ziwei Liu. Lgm: Large multi-view gaussian model for high-resolution 3d content creation. *arXiv preprint arXiv:2402.05054*, 2024. 3
- KLING AI Team. Kling image-to-video model, 2024. URL <https://klingai.com/image-to-video/>. 6, 8, 20
- Zachary Teed and Jia Deng. Raft: Recurrent all-pairs field transforms for optical flow. In *European conference on computer vision*, pp. 402–419. Springer, 2020. 7
- Sergey Tulyakov, Ming-Yu Liu, Xiaodong Yang, and Jan Kautz. Mocogan: Decomposing motion and content for video generation. In *Proceedings of the IEEE conference on computer vision and pattern recognition*, pp. 1526–1535, 2018. 3
- Thomas Unterthiner, Sjoerd Van Steenkiste, Karol Kurach, Raphaël Marinier, Marcin Michalski, and Sylvain Gelly. Fvd: A new metric for video generation. 2019. 8
- Carl Vondrick, Hamed Pirsiavash, and Antonio Torralba. Generating videos with scene dynamics. *Advances in neural information processing systems*, 29, 2016. 3

- Team Wan, Ang Wang, Baole Ai, Bin Wen, Chaojie Mao, Chen-Wei Xie, Di Chen, Fei Wu, Haiming Zhao, Jianxiao Yang, et al. Wan: Open and advanced large-scale video generative models. *arXiv preprint arXiv:2503.20314*, 2025. 3, 7, 9, 10, 18, 20
- Chaoyang Wang, Peiye Zhuang, Tuan Duc Ngo, Willi Menapace, Aliaksandr Siarohin, Michael Vasilkovsky, Ivan Skorokhodov, Sergey Tulyakov, Peter Wonka, and Hsin-Ying Lee. 4real-video: Learning generalizable photo-realistic 4d video diffusion. In *Proceedings of the Computer Vision and Pattern Recognition Conference*, pp. 17723–17732, 2025a. 3
- Jianyuan Wang, Minghao Chen, Nikita Karaev, Andrea Vedaldi, Christian Rupprecht, and David Novotny. Vggg: Visual geometry grounded transformer. In *Proceedings of the Computer Vision and Pattern Recognition Conference*, pp. 5294–5306, 2025b. 19, 24
- Qianqian Wang, Vickie Ye, Hang Gao, Jake Austin, Zhengqi Li, and Angjoo Kanazawa. Shape of motion: 4d reconstruction from a single video. *arXiv preprint arXiv:2407.13764*, 2024a. 23
- Yaohui Wang, Piotr Bilinski, Francois Bremond, and Antitza Dantcheva. Imaginator: Conditional spatio-temporal gan for video generation. In *Proceedings of the IEEE/CVF winter conference on applications of computer vision*, pp. 1160–1169, 2020. 3
- Yaohui Wang, Xinyuan Chen, Xin Ma, Shangchen Zhou, Ziqi Huang, Yi Wang, Ceyuan Yang, Yinan He, Jiashuo Yu, Peiqing Yang, et al. Lavie: High-quality video generation with cascaded latent diffusion models. *IJCV*, 2024b. 3
- Yiran Wang, Min Shi, Jiaqi Li, Zihao Huang, Zhiguo Cao, Jianming Zhang, Ke Xian, and Guosheng Lin. Neural video depth stabilizer. In *Proceedings of the IEEE/CVF International Conference on Computer Vision*, pp. 9466–9476, 2023. 6, 20
- Zhou Wang, Alan C Bovik, Hamid R Sheikh, and Eero P Simoncelli. Image quality assessment: from error visibility to structural similarity. *IEEE TIP*, 13(4):600–612, 2004. 8
- Zhouxia Wang, Ziyang Yuan, Xintao Wang, Yaowei Li, Tianshui Chen, Menghan Xia, Ping Luo, and Ying Shan. Motionctrl: A unified and flexible motion controller for video generation. In *ACM SIGGRAPH 2024 Conference Papers*, pp. 1–11, 2024c. 3
- Chenfei Wu, Lun Huang, Qianxi Zhang, Binyang Li, Lei Ji, Fan Yang, Guillermo Sapiro, and Nan Duan. Godiva: Generating open-domain videos from natural descriptions. *arXiv preprint arXiv:2104.14806*, 2021. 3
- Chenfei Wu, Jian Liang, Lei Ji, Fan Yang, Yuejian Fang, Daxin Jiang, and Nan Duan. Nüwa: Visual synthesis pre-training for neural visual world creation. In *ECCV*, pp. 720–736, 2022. 3
- Rundi Wu, Ruiqi Gao, Ben Poole, Alex Trevithick, Changxi Zheng, Jonathan T Barron, and Aleksander Holynski. Cat4d: Create anything in 4d with multi-view video diffusion models. In *Proceedings of the Computer Vision and Pattern Recognition Conference*, pp. 26057–26068, 2025. 3
- Zeqi Xiao, Wenqi Ouyang, Yifan Zhou, Shuai Yang, Lei Yang, Jianlou Si, and Xingang Pan. Trajectory attention for fine-grained video motion control. *arXiv preprint arXiv:2411.19324*, 2024. 3
- Jinbo Xing, Menghan Xia, Yong Zhang, Haoxin Chen, Wangbo Yu, Hanyuan Liu, Xintao Wang, Tien-Tsin Wong, and Ying Shan. Dynamicrafter: Animating open-domain images with video diffusion priors. *arXiv preprint arXiv:2310.12190*, 2023. 3, 5
- Jinbo Xing, Menghan Xia, Yuxin Liu, Yuechen Zhang, Yong Zhang, Yingqing He, Hanyuan Liu, Haoxin Chen, Xiaodong Cun, Xintao Wang, et al. Make-your-video: Customized video generation using textual and structural guidance. *IEEE Transactions on Visualization and Computer Graphics*, 2024. 3
- Shiyuan Yang, Liang Hou, Haibin Huang, Chongyang Ma, Pengfei Wan, Di Zhang, Xiaodong Chen, and Jing Liao. Direct-a-video: Customized video generation with user-directed camera movement and object motion. In *ACM SIGGRAPH 2024 Conference Papers*, pp. 1–12, 2024a. 3

- Zhuoyi Yang, Jiayan Teng, Wendi Zheng, Ming Ding, Shiyu Huang, Jiazheng Xu, Yuanming Yang, Wenyi Hong, Xiaohan Zhang, Guanyu Feng, et al. Cogvideox: Text-to-video diffusion models with an expert transformer. *arXiv preprint arXiv:2408.06072*, 2024b. [3](#), [8](#), [20](#)
- Chongjie Ye, Yushuang Wu, Ziteng Lu, Jiahao Chang, Xiaoyang Guo, Jiaqing Zhou, Hao Zhao, and Xiaoguang Han. Hi3dgen: High-fidelity 3d geometry generation from images via normal bridging. *arXiv preprint arXiv:2503.22236*, 2025. [3](#)
- Shengming Yin, Chenfei Wu, Jian Liang, Jie Shi, Houqiang Li, Gong Ming, and Nan Duan. Dragnuwa: Fine-grained control in video generation by integrating text, image, and trajectory. *arXiv preprint arXiv:2308.08089*, 2023. [3](#)
- Meng You, Zhiyu Zhu, Hui Liu, and Junhui Hou. Nvs-solver: Video diffusion model as zero-shot novel view synthesizer. In *International Conference on Learning Representations*, 2025. [3](#)
- Mark YU, Wenbo Hu, Jinbo Xing, and Ying Shan. Trajectorycrafter: Redirecting camera trajectory for monocular videos via diffusion models. *arXiv preprint arXiv:2503.05638*, 2025. [2](#), [3](#), [4](#), [5](#), [7](#), [8](#), [18](#), [20](#), [21](#), [23](#), [24](#), [25](#)
- Wangbo Yu, Jinbo Xing, Li Yuan, Wenbo Hu, Xiaoyu Li, Zhipeng Huang, Xiangjun Gao, Tien-Tsin Wong, Ying Shan, and Yonghong Tian. Viewcrafter: Taming video diffusion models for high-fidelity novel view synthesis. *arXiv preprint arXiv:2409.02048*, 2024. [3](#), [4](#), [25](#)
- Jianshu Zeng, Yuxuan Liu, Yutong Feng, Chenxuan Miao, Zixiang Gao, Jiawang Qu, Jianzhang Zhang, Bin Wang, and Kun Yuan. Lumen: Consistent video relighting and harmonious background replacement with video generative models. *arXiv preprint arXiv:2508.12945*, 2025. [3](#)
- David Junhao Zhang, Roni Paiss, Shiran Zada, Nikhil Karnad, David E Jacobs, Yael Pritch, Inbar Mosseri, Mike Zheng Shou, Neal Wadhwa, and Nataniel Ruiz. Recapture: Generative video camera controls for user-provided videos using masked video fine-tuning. In *Proceedings of the Computer Vision and Pattern Recognition Conference*, pp. 2050–2062, 2025a. [2](#), [3](#)
- Lvmin Zhang, Anyi Rao, and Maneesh Agrawala. Scaling in-the-wild training for diffusion-based illumination harmonization and editing by imposing consistent light transport. In *The Thirteenth International Conference on Learning Representations*, 2025b. [2](#), [3](#), [4](#), [6](#), [7](#), [8](#), [9](#), [10](#), [18](#), [19](#), [20](#), [23](#), [26](#), [30](#)
- Richard Zhang, Phillip Isola, Alexei A Efros, Eli Shechtman, and Oliver Wang. The unreasonable effectiveness of deep features as a perceptual metric. In *CVPR*, pp. 586–595, 2018. [8](#)
- Shiwei Zhang, Jiayu Wang, Yingya Zhang, Kang Zhao, Hangjie Yuan, Zhiwu Qin, Xiang Wang, Deli Zhao, and Jingren Zhou. I2vgen-xl: High-quality image-to-video synthesis via cascaded diffusion models. *arXiv preprint arXiv:2311.04145*, 2023. [18](#)
- Guangcong Zheng, Teng Li, Rui Jiang, Yehao Lu, Tao Wu, and Xi Li. Cami2v: Camera-controlled image-to-video diffusion model. *arXiv preprint arXiv:2410.15957*, 2024. [3](#)
- Sixiao Zheng, Zimian Peng, Yanpeng Zhou, Yi Zhu, Hang Xu, Xiangru Huang, and Yanwei Fu. Vidcraft3: Camera, object, and lighting control for image-to-video generation. *arXiv preprint arXiv:2502.07531*, 2025. [3](#)
- Daquan Zhou, Weimin Wang, Hanshu Yan, Weiwei Lv, Yizhe Zhu, and Jiashi Feng. Magicvideo: Efficient video generation with latent diffusion models. *arXiv preprint arXiv:2211.11018*, 2022. [3](#)
- Hao Zhou, Sunil Hadap, Kalyan Sunkavalli, and David W Jacobs. Deep single-image portrait relighting. In *Proceedings of the IEEE/CVF international conference on computer vision*, pp. 7194–7202, 2019. [3](#)
- Yujie Zhou, Jiazi Bu, Pengyang Ling, Pan Zhang, Tong Wu, Qidong Huang, Jinsong Li, Xiaoyi Dong, Yuhang Zang, Yuhang Cao, et al. Light-a-video: Training-free video relighting via progressive light fusion. *arXiv preprint arXiv:2502.08590*, 2025. [2](#), [3](#), [7](#), [8](#), [9](#), [18](#), [19](#), [20](#), [21](#), [23](#), [27](#)

A MORE IMPLEMENTATION DETAILS

A.1 TRAINING-FREE BASELINE: TL-FREE

The baseline method TL-Free is inspired by Light-A-Video (LAV) (Zhou et al., 2025), which integrates TrajectoryCrafter (YU et al., 2025) and IC-Light (Zhang et al., 2025b) in a training-free manner. LAV introduces three key components: consistent light attention, progressive light fusion, and details compensation, to achieve temporally coherent video relighting. However, unlike LAV, which directly processes original video frames for relighting, our objective is to simultaneously perform relighting and camera viewpoint changes. Thus, the model input is not the raw video but point-cloud projected views, which are geometrically aligned yet inevitably contain black borders and holes. This critical difference necessitates adapting the LAV modules as follows: **1) Details compensation.** While effective in LAV for enhancing frame-level fidelity, this module relies on the input video to supplement missing details. For our projected views, however, it propagates black borders and holes, severely degrading the results. We thus discard this module in TL-Free. **2) Progressive light fusion.** In LAV, the fusion ratio between IC-Light and the video diffusion backbone is controlled by a schedule: IC-Light dominates early denoising steps and gradually diminishes. For our projected views, applying IC-Light early is problematic, since relighting images with black borders or incomplete regions is ill-posed. We therefore disable IC-Light fusion during early denoising and only activate it in later steps, once the model has filled in missing content. **3) Consistent light attention.** This module is retained, as it ensures temporally consistent illumination across frames and remains effective even when operating on projected views.

A.2 BACKGROUND-CONDITIONED CONTROL

As shown in Fig. A, our framework supports background-conditioned video relighting. Specifically, the source video V^s is obtained by fusing a foreground video with a background video using foreground masks. IC-Light (Zhang et al., 2025b) is then applied to generate a sparse relit video \hat{V}^s , which provides illumination cues. Finally, both V^s and \hat{V}^s are fed into our model to produce the relit video with consistent illumination and motion.

A.3 BASELINE

For Light-A-Video (LAV) (Zhou et al., 2025), we adopt the officially released Wan2.1 (Wan et al., 2025) implementation and use the default hyperparameter settings. For AnyV2V (Ku et al., 2024), we evaluate the officially released model built on I2VGen-XL (Zhang et al., 2023) under its default configuration. The released model generates 16-frame videos at a resolution of 512×512 . For RelightVid (Fang et al., 2025), as it currently only provides a background-image-conditioned model without text-conditioned variants or training code, we evaluate it exclusively under the background-conditioned setting using the official model released by the authors. Its outputs also have 16 frames with a spatial resolution of 512×512 . For fair comparison, all baseline outputs are uniformly resized to match the resolution adopted in our evaluation.

A.4 EVALUATION PROTOCOL AND USER STUDY

Evaluation Protocol. For text-conditioned relighting, we randomly select one lighting prompt (e.g., sunlight, soft light, neon light, or red and blue neon light) and one lighting direction (top, bottom, left, or right) for each video. For novel-view video generation, one of four predefined camera trajectories is randomly chosen. After the condition is determined, we apply the same lighting prompt and camera trajectory to all methods to ensure fair comparison. In the joint camera-illumination control evaluation, we first employ TrajectoryCrafter (YU et al., 2025) to generate the novel-view sequence. This sequence is then compared against relit sequences produced by other methods under the same trajectory to compute the flow error (i.e., Motion Preservation). Additionally, we apply IC-Light (Zhang et al., 2025b) to relight the novel-view video from TrajectoryCrafter, which serves as the reference for calculating FID with respect to the relit outputs of all baselines.

User Study. We conducted a user study to evaluate the effectiveness of our method across three tasks: 1) joint camera-illumination control, 2) text-conditioned video relighting, and 3) background-conditioned video relighting. The study was conducted online, and screenshots of the interface

are shown in Fig. B. The interface displayed the input video, the corresponding relighting prompt (text or background image), and two relit results (denoted as Method 1 and Method 2) side by side. Participants could play both videos in parallel and directly compare their quality. On the left panel, four criteria were listed with radio buttons for selection: Relighting Quality (RQ, lighting fidelity, and alignment with the condition), Video Smoothness (VS, temporal stability across frames), Identity Preservation (IP, consistency of the object’s identity and appearance), and 4D Consistency (4DC, spatio-temporal coherence under novel-view settings). For each criterion, participants were required to select which method performed better. They were also allowed to choose “Hard to judge” or skip to the next example if necessary. To reduce fatigue and ensure reliable feedback, the system required participants to submit responses after completing 10 groups of comparisons. The study was conducted anonymously, and no personally identifiable data were collected. In total, we collected responses from 57 participants.

B DETAILED DATA CURATION

Training Data Requirements Analysis. As discussed in Sec. 3.3 in the main text, training our framework requires an input video V^s , a paired target video V^t , and conditioning sequences V^p , \hat{V}^s , and \hat{V}^p . To ensure effective training, these modalities should satisfy the following requirements:

- **Target video V^t .** Serving as the ground truth, the target video should be of high visual quality and exhibit temporal consistency.
- **Input video V^s .** Serving as the reference sequence injected into the network, the input video should remain 4D-consistent with the target video V^t in their overlapping regions.
- **Projected source views V^p .** Serving as a geometric view-transformation prior, these projections should maintain content consistency with the target video V^t in shared visible regions.
- **Sparse relit video \hat{V}^s .** Serving as an explicit lighting prior for the diffusion model, the relit frame should share the same illumination as the target video V^t .
- **Projected relit views \hat{V}^p .** Serving as fine-grained illumination cues, these projections should be geometrically aligned with the corresponding projected source views V^p , ensuring that illumination information is accurately fused with the geometric prior.

Pipeline Design. As shown in Fig. C, we design a degradation-based pipeline to construct paired videos based on these requirements. Specifically, we treat an in-the-wild video as the target sequence V^t and generate its degraded counterpart as the input sequence V^s to satisfy the above constraints. Furthermore, by recording the transformations applied during the degradation process, we apply their inverses to map the geometry and illumination of the target video back to the degraded sequence, thereby producing the corresponding conditioning cues V^p , \hat{V}^s and \hat{V}^p that conform to the training requirements and enable training with the degraded video as input.

Data Sources. We curate training pairs from three complementary sources:

- **Static scenes.** Monocular videos of static scenes naturally provide multi-view observations of the same scene. We adopt two strategies to construct paired samples with only varied viewpoints: 1) sample a video clip as one view and create the other by repeating a randomly selected frame from the same sequence; 2) select two clips with overlapping content as a pair. For both cases, we employ VGGT (Wang et al., 2025b) to reconstruct depths and camera poses, thereby establishing the geometric transformations between views. To further introduce illumination variation, we process the data according to the pairing type: 1) relight the image-repeated video using IC-Light (Zhang et al., 2025b), which serves as the degraded input V^s while naturally maintaining temporal consistency due to the repeated frames, and take the other video as V^t ; 2) relight one clip with Light-A-Video (LAV) (Zhou et al., 2025), treating the relit clip as V^s and the remaining clip as V^t . Although the latter approach yields slightly weaker temporal consistency, it still preserves the scene content and meets our data requirements. Finally, leveraging the geometric transformations estimated by (Wang et al., 2025b), we warp the information in V^s to the viewpoint of V^t , thereby constructing the data required for training. With this approach, we curate 8k static training samples from the DL3DV (Ling et al., 2024) dataset.

- **Dynamic scenes.** Given a dynamic monocular video V^t , we construct degraded counterparts V^s using three strategies: 1) relight V^t with Light-A-Video (Zhou et al., 2025) and then synthesize a novel-view video V^s via TrajectoryCrafter (YU et al., 2025); 2) synthesize a novel-view video using (YU et al., 2025) and then apply (Zhou et al., 2025) to introduce illumination variations, producing V^s . 3) directly generate a relit and novel-view video V^s through our designed training-free pipeline TL-Free (details are provided in the Sec. A.1). The degraded videos V^s produced by these strategies are used as inputs for model training. Although their temporal consistency and visual quality are not perfect, they satisfy our data requirements, such as maintaining content consistency with the target video V^t in overlapping regions. To ensure geometric alignment, all warping operations rely on depths estimated once from the original video rather than being re-estimated from intermediate results. During degradation, we derive the correspondence flow $F_{t \rightarrow s}$ from the depth and relative pose and warp the original frame to the degraded view. When constructing the training set, we then apply the reverse flow $F_{s \rightarrow t}$ to warp the degraded samples back to the original viewpoint, thereby obtaining geometrically aligned conditions. Using this procedure, we curate 8k dynamic training samples from the VDW (Wang et al., 2023) dataset.
- **AI-generated videos.** While the above methods use high-quality real-world videos as supervision, most videos exhibit relatively uniform and soft lighting, limiting the diversity of illumination conditions. To address this, we design a data pipeline based on commercial video generation models to synthesize videos with richer lighting variations. Specifically, we first employ (YU et al., 2025) to generate a novel-view video from the original sequence V^t , then extract its first frame and relight it using (Zhang et al., 2025b). The relit frame, together with the novel-view video, is fed into the first-frame-guided video-to-video mode of a commercial generative model (e.g., Runway or Luma) to produce a relit video, resulting in the paired video V^s . This approach yields videos with diverse illumination while maintaining high temporal consistency, thanks to the commercial model’s powerful capability. For this set of data, we follow the standard training strategy, using V^t as the input and V^s as the target video. However, a limitation of this approach is that, although it ensures temporal consistency, the commercial model tends to generate content inconsistent with the original video when the scene or camera motion is relatively large, violating the data requirements discussed above and adversely affecting the learning of our model. Therefore, we only retain videos with small motion, which we identify and filter using an optical-flow-based criterion (Huang et al., 2024), and we ultimately curate 2k samples from the OpenVid-1M (Nan et al., 2024) dataset.

Together, the three data sources provide complementary training pairs for our framework: static scenes offer accurate multi-view data, dynamic scenes supply samples with scene motion, and AI-generated videos enrich illumination diversity. All of them satisfy the training requirements, providing paired inputs, targets, and geometrically aligned conditioning cues.

C PRELIMINARY: VIDEO DIFFUSION MODELS

Video diffusion models consist of two stages: a forward process and a reverse process. The forward process starts from clean video data $\mathbf{x}_0 \in \mathbb{R}^{f \times 3 \times h \times w}$ and gradually injects noise to create noisy states as $\mathbf{x}_t = \alpha_t \mathbf{x}_0 + \sigma_t \epsilon$, where $\epsilon \sim \mathcal{N}(\mathbf{0}, \mathbf{I})$ and $\alpha_t^2 + \sigma_t^2 = 1$. The reverse process removes noise with a predictor $\epsilon_\theta(\mathbf{x}_t, t)$, optimized by

$$\min_{\theta} \mathbb{E}_{t \sim \mathcal{U}(0,1), \epsilon \sim \mathcal{N}(\mathbf{0}, \mathbf{I})} [\|\epsilon_\theta(\mathbf{x}_t, t) - \epsilon\|_2^2]. \quad (8)$$

For computational efficiency, videos are first compressed into latents $\mathbf{z} = \mathcal{E}(\mathbf{x})$ using a pre-trained 3D VAE (Kingma & Welling, 2013; Rombach et al., 2022). The latents are then patchified, concatenated with text embeddings, and fed into the noise estimator. Recent works (Yang et al., 2024b; Wan et al., 2025; Lin et al., 2024; Kong et al., 2024; Brooks et al., 2024; Team, 2024) commonly adopt the Diffusion Transformer (DiT) (Peebles & Xie, 2023) as the noise estimator, owing to its strong modeling capacity and flexible scalability. During inference, noisy latents are iteratively denoised, then reconstructed by the VAE decoder to produce the final video $\hat{\mathbf{x}} = \mathcal{D}(\mathbf{z})$.

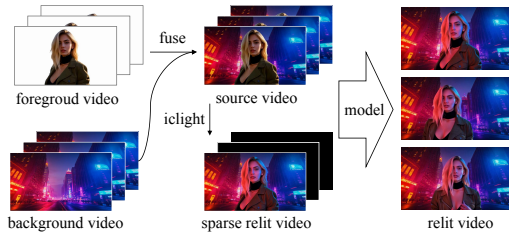


Figure A: Overview of background-conditioned video relighting. A foreground video is fused with a background video to form the source video, while IC-Light generates a sparse relit video. Both are fed into our model to produce the final relit video with consistent illumination and motion.

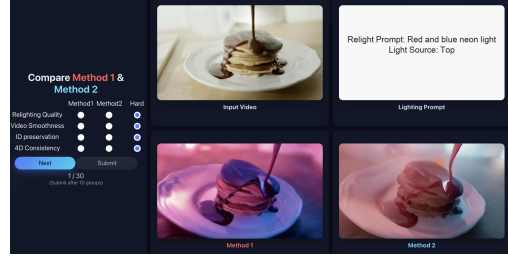


Figure B: The web interface of our user studies. Participants were shown the input video, the relighting prompt (text or background image), and results of two methods (Method 1 and Method 2) side by side. They evaluated each pair across four criteria by selecting the better method.

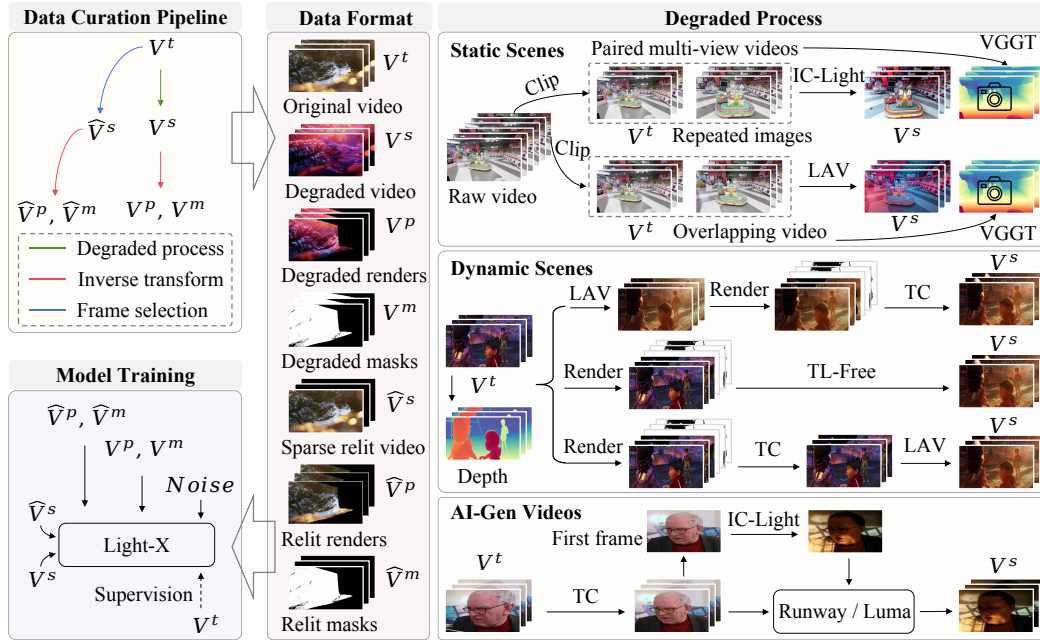


Figure C: Detailed Data curation pipeline **Light-Syn**. Given an original in-the-wild video V^t , we synthesize a degraded counterpart V^s using different strategies for static, dynamic, and AI-generated scenes. From V^s , we obtain geometry-aligned renders and masks (V^p, V^m) and relit counterparts (\hat{V}^p, \hat{V}^m) via inverse geometric transformations. The curated data provide paired videos for training, with Light-X taking the degraded video as input, the other signals as conditions, and the original video as ground truth.

D MORE EXPERIMENTAL RESULTS

D.1 ADDITIONAL RESULTS ON CAMERA-ILLUMINATION CONTROL

Additional Visual Comparisons. Fig. Q presents further results on joint camera-illumination control. TC (YU et al., 2025)+LAV (Zhou et al., 2025) inherits the limited relighting capacity of LAV, which becomes particularly fragile under large camera motion, leading to distorted illumination and unstable temporal transitions. When LAV is applied after TC, the relit results undermine the geometric reconstruction, causing TC to introduce noticeable artifacts in novel views. TL-Free, on the other hand, fails to balance fidelity and consistency, often yielding either excessively simplified

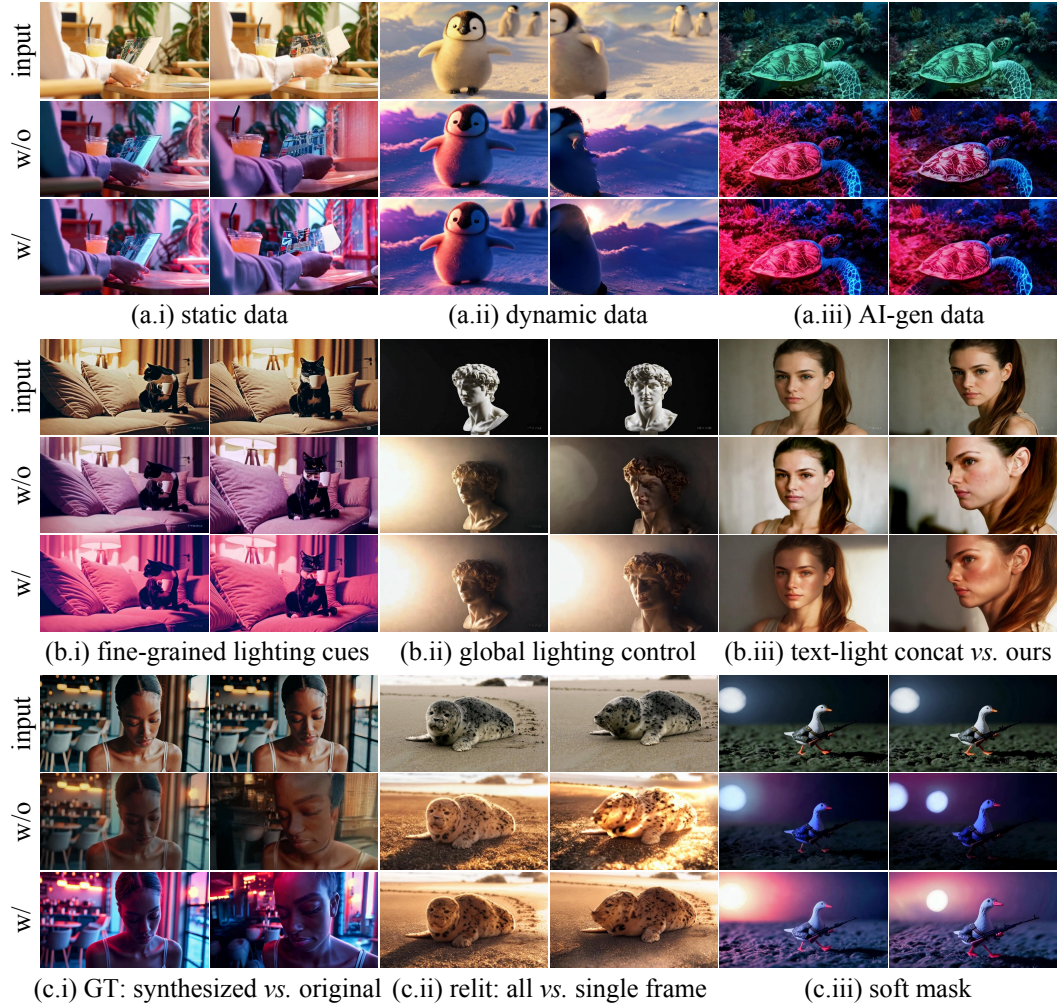


Figure D: Qualitative ablation results for the joint camera-illumination control task.

Table A: Quantitative comparison with baseline methods for joint camera-illumination control on the iPhone (Gao et al., 2022) multi-view dataset.

Method	FID ↓	Aesthetic ↑	Motion Preservation ↓	CLIP ↑
Target-view video + IC-Light	/	0.571	5.412	0.973
TrajectoryCrafter + Light-A-Video	236.57	0.516	5.757	0.987
Light-A-Video + TrajectoryCrafter	218.72	0.520	4.620	0.986
TL-Free	198.55	0.488	6.428	0.985
Ours	155.36	0.557	3.316	0.987

Table B: Quantitative comparison of video relighting under HDR-map conditioning.

Method	PSNR ↑	SSIM ↑	LPIPS ↓	Consistency (Temp. / Subj. / Backg.) ↑	Motion Smooth. ↑	Aesthetics (Qual. / Img.) ↑
DiffusionRenderer	11.88	0.4510	0.4931	0.9921 / 0.9560 / 0.9599	0.9944	0.5262 / 0.4495
Ours	16.98	0.6653	0.2504	0.9933 / 0.9608 / 0.9676	0.9927	0.5909 / 0.6277

lighting effects or severe temporal flickering. In contrast, our method achieves high-quality relighting

under diverse lighting prompts (*e.g.*, neon, soft, sunlight) while preserving temporal consistency and realistic novel-view content generation, consistently outperforming baseline methods.

Results on iPhone Multi-view Dataset. We further adopt the iPhone dataset (Gao et al., 2022), which contains 7 dynamic scenes captured with a casually moving camera and two static cameras. Following prior work (YU et al., 2025; Wang et al., 2024a), we discard the “Space-out” and “Wheel” scenes due to camera and LiDAR errors, and use the remaining 5 refined scenes, namely *Apple*, *Block*, *Paper*, *Spin*, and *Teddy*. These data provide multi-view videos of the same dynamic scenes, serving as a valuable benchmark for assessing novel-view content generation with or without relighting. In our evaluation, the casually moving camera videos are used as input to synthesize target static-camera views with relighting, while the ground-truth static-camera videos serve as references for computing motion preservation. For FID computation, we relight the ground-truth static-camera videos using IC-Light (Zhang et al., 2025b) as the reference. As shown in Table A, our method achieves the best overall performance on this dataset. In particular, it attains the lowest FID, indicating superior visual fidelity, and significantly improves motion preservation compared to baselines. Although IC-Light applied to target-view videos yields a slightly higher aesthetic score, since it does not require novel-view generation, our approach achieves a better overall balance across all metrics, consistently outperforming baselines in relighting quality, temporal stability, and novel-view generation.

D.2 ADDITIONAL RESULTS ON TEXT-CONDITIONED RELIGHTING

We provide more qualitative results of text-conditioned video relighting in Fig. R. Frame-wise IC-Light (Zhang et al., 2025b) delivers high-quality relighting on individual frames, but the absence of temporal modeling leads to noticeable flickering across videos. LAV (Zhou et al., 2025) leverages video diffusion priors through a training-free fusion strategy, which improves temporal stability but often compromises lighting fidelity and detail. In contrast, our method achieves high-quality and consistent video relighting under diverse lighting prompts while preserving temporal consistency, consistently outperforming baseline methods.

D.3 ADDITIONAL RESULTS ON BACKGROUND-CONDITIONED RELIGHTING

We further present qualitative comparisons of background image-conditioned video relighting in Fig. E. IC-Light (Zhang et al., 2025b) often produces inconsistent illumination across frames due to its frame-wise nature, resulting in flickering and mismatched tones. RelightVid (Fang et al., 2025) improves temporal stability but tends to over-smooth the lighting effects, leading to a loss of realism. LAV (Zhou et al., 2025) enhances consistency but sacrifices fine details, producing less faithful relighting results. In contrast, our method effectively integrates the subject with the target background illumination, achieving natural lighting and temporally stable outputs. As shown in Fig. F, our framework generalizes well to diverse background images, adapting the relighting smoothly while preserving subject identity and fine-grained details.

D.4 ADDITIONAL RESULTS ON HDR MAP-CONDITIONED RELIGHTING

We further present qualitative results of HDR map-conditioned video relighting in Fig. S. Given an input video and an HDR environment map, our model generates plausible relit videos that faithfully reflect the target illumination, demonstrating the potential of our soft-mask design to adapt to diverse lighting conditions. To quantitatively evaluate this setting, we also compare against DiffusionRenderer (Liang et al., 2025). Since no paired in-the-wild dataset is available, we adopt a strategy similar to our data curation pipeline. Specifically, for each in-the-wild video in the evaluation set, we extract HDR maps using DiffusionLight (Phongthawee et al., 2024), and use Light-a-Video (Zhou et al., 2025) to produce aligned relit videos. These relit videos are then used as model inputs, while the extracted HDR maps serve as conditions. We compute metrics (*e.g.*, PSNR, SSIM, LPIPS) between the model outputs and the original in-the-wild videos, where our approach achieves superior scores. However, this evaluation setting inherently favors our training paradigm. To provide a more balanced assessment, we further evaluate video quality on VBench (Huang et al., 2024). The results show that our outputs are comparable to DiffusionRenderer in terms of overall visual quality, demonstrating the generalization ability of our framework to diverse lighting conditions and the potential of HDR maps as a versatile control signal.



Figure E: Qualitative comparison of background image-conditioned video relighting. Our method achieves superior both relighting quality and temporal consistency compared to baseline methods.

D.5 ADDITIONAL RESULTS ON REFERENCE IMAGE-CONDITIONED RELIGHTING

We present the results of reference image-conditioned video relighting in Fig. T, where a single reference image specifies the target illumination style to be transferred to the input video. To the best of our knowledge, our framework is the first to enable this setting. Furthermore, as shown in Fig. U, our approach also supports simultaneous relighting and novel-view synthesis, achieving both illumination control and camera trajectory manipulation.

D.6 ADDITIONAL RESULTS ON NOVEL VIEW SYNTHESIS

To further evaluate novel-view video generation, we compare our method with TrajectoryCrafter (YU et al., 2025) on the multi-view iPhone (Gao et al., 2022) dataset. As shown in Table C, our method achieves higher PSNR and lower LPIPS, while maintaining comparable SSIM. This suggests that our framework performs on par with its baseline method in novel-view video synthesis, while providing additional flexibility for joint camera–illumination control.

Table C: Quantitative comparison between our method and TrajectoryCrafter (YU et al., 2025) on the iPhone (Gao et al., 2022) dataset.

Method	PSNR \uparrow	SSIM \uparrow	LPIPS \downarrow
TrajectoryCrafter	14.6204	0.5725	0.3801
Ours	15.6016	0.5696	0.3519

D.7 GEOMETRY CONSISTENCY EVALUATION

To further validate the geometric coherence of our relighting results, we conduct a comprehensive point-cloud-based evaluation. Specifically, we reconstruct dynamic and static 3D geometry from both the input and relighted videos using two state-of-the-art methods: the dynamic reconstruction method MegaSAM (Li et al., 2025b) and the static reconstruction model VGGT (Wang et al., 2025b). For each video, we extract per-frame point clouds and compute the Chamfer Distance (CD) between the input and relighted reconstructions. We report multiple statistics, including *Mean*, *Median*, *Standard Deviation*, *Minimum*, and *Maximum* Chamfer Distance (CD), to provide a comprehensive assessment of geometric discrepancies. As shown in Table D, our method achieves the lowest mean and median CD, demonstrating substantially better preservation of geometric structure. Qualitative point cloud visualizations are included in the supplementary video.



Figure F: Visual results of background image-conditioned video relighting. Our method adapts the foreground subject to diverse background images, producing natural illumination and consistent appearance across frames.

Table D: Geometry consistency evaluation. Chamfer Distance (CD) between point clouds reconstructed from the input and relighted videos. * denotes evaluation on the first 16 frames.

Method	Avg CD ↓	Median ↓	Std ↓	Min ↓	Max ↓
IC-Light	0.5012	0.1933	1.3300	0.0056	15.6113
LAV	0.8979	0.1903	4.5258	0.0096	58.0839
Ours	0.3753	0.1581	0.7228	0.0063	5.9780
IC-Light + AnyV2V	0.8896	0.2813	1.8282	0.0055	19.9080
Ours*	0.3784	0.1577	0.7535	0.0064	5.8883

D.8 ANALYSIS ON NON-LAMBERTIAN SURFACES

As shown in Fig. G, we present additional results on non-Lambertian surfaces, showing that the model preserves specular effects without washing out fine details. The corresponding video results are provided in the supplementary video.

D.9 LARGE CAMERA TRAJECTORIES

Similar to other approaches (Yu et al., 2024; YU et al., 2025; Liu et al., 2025a) that condition on point-cloud priors, our method relies on point-cloud cues to guide viewpoint-consistent generation. Under extremely wide camera motions, these cues become sparse or even unavailable, which can

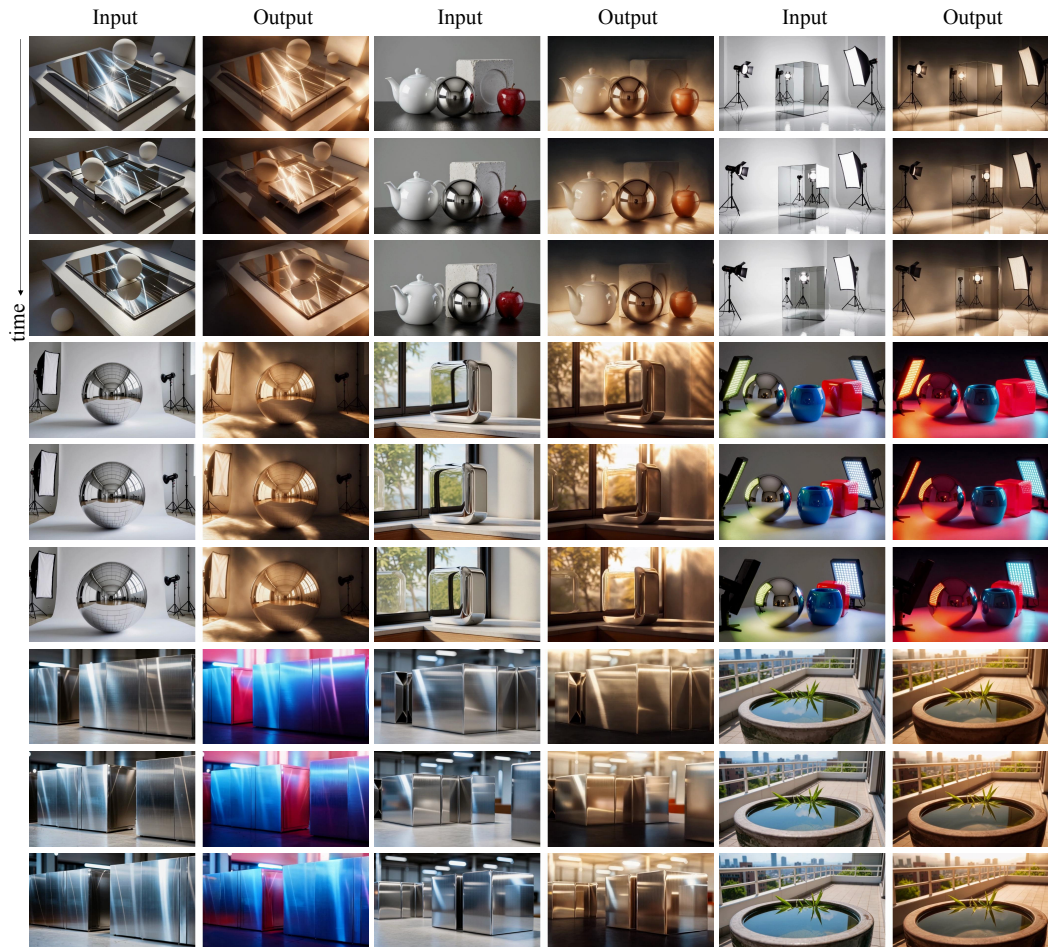


Figure G: Results on non-Lambertian surfaces.

negatively affect synthesis quality. Nevertheless, the model remains robust under substantial viewpoint deviations, roughly up to 60° , as shown in Fig. H. The corresponding video results are provided in the supplementary video.

D.10 COMPARISON WITH MORE RECENT METHODS

We further compare Light-X with several recent systems that provide either camera control or lighting control capabilities, covering the latest advances in controllable video generation. For camera control, we include ReCamMaster (Bai et al., 2025), which does not rely on explicit 3D representations, and Free4D (Liu et al., 2025a), which incorporates an explicit 3D representation. For lighting control, we further compare against TC-Light (Liu et al., 2025b). The results for joint camera-illumination control and video relighting are reported in Tables E and F. Across all comparisons, Light-X maintains superior image fidelity, aesthetic quality, and motion consistency, demonstrating strong state-of-the-art performance even against these recent systems. Since Free4D requires per-scene optimization, typically taking over an hour per scene, we evaluate it on the 10 scenes provided on its official project page for practical comparison. The corresponding results are shown in Table G.

D.11 FID DEGRADATION WITH TEMPORAL DISTANCE

We analyze how FID changes with increasing temporal distance from the relit reference frame. As shown in Fig. J, FID gradually increases because it is computed against the IC-Light (Zhang et al.,

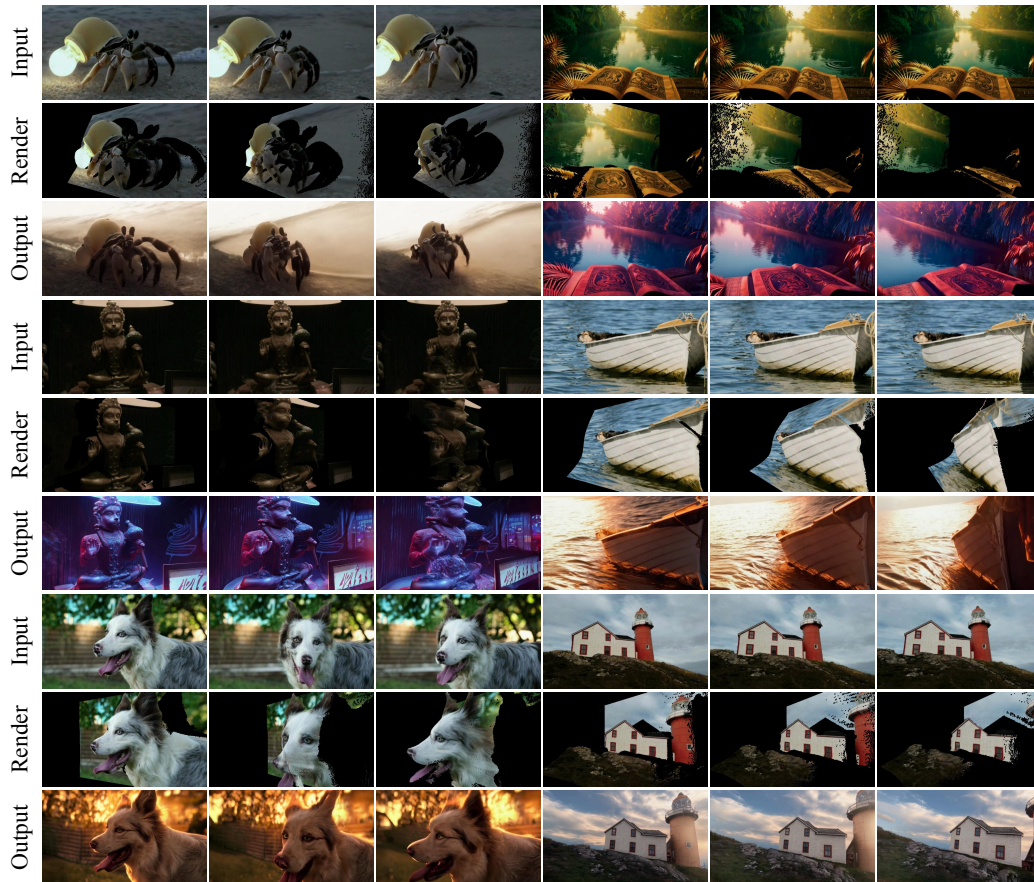


Figure H: Qualitative results under large camera trajectories.

Table E: Comparison with more recent methods for joint camera-illumination control.

Method	FID ↓	Aesthetic ↑	Motion Pres. ↓	CLIP ↑
TC + IC-Light	/	0.573	6.558	0.976
TC + LAV	138.89	0.574	4.327	0.986
LAV + TC	144.61	0.596	5.027	0.987
TL-Free	122.73	0.595	3.356	0.987
ReCam + IC-Light	/	0.513	6.511	0.973
LAV + ReCam	163.56	0.514	7.259	0.989
ReCam + LAV	152.03	0.501	3.157	0.987
TC + TC-Light	154.99	0.534	4.276	0.986
TC-Light + TC	161.76	0.555	5.563	0.988
Ours	101.06	0.623	2.007	0.989

2025b) relit reference: the first frame is directly relit by IC-Light, whereas later frames rely on Light-X to propagate illumination cues over time.

For video relighting, FID increases smoothly from 38 to 82 over 49 frames. For joint camera-illumination control, FID rises from 56 to 100. Importantly, even the last frame still outperforms baseline methods such as LAV (Zhou et al., 2025) (FID: 112.45) and TL-Free (FID: 122.73).

Table F: Comparison with more recent lighting control methods on video relighting.

Method	FID ↓	Aesthetic ↑	Motion Pres. ↓	CLIP ↑
IC-Light	/	0.632	3.293	0.983
LAV	112.45	0.614	2.115	0.991
TC-Light	144.32	0.546	1.657	0.991
Ours	83.65	0.645	1.137	0.993

Table G: Evaluation results on the 10 scenes released on the Free4D (Liu et al., 2025a) project page.

Method	FID ↓	Aesthetic ↑	Motion Pres. ↓	CLIP ↑
Free4D + IC-Light	/	0.576	0.823	0.990
Free4D + LAV	98.85	0.574	0.549	0.996
Ours	73.98	0.583	0.349	0.997

D.12 PERFORMANCE WITH OCCLUDED RELIT FRAMES

As shown in Fig. I, Light-X remains robust even when the relit reference frame (the first frame in the illustrated example) is partially occluded or contains incomplete scene information. Illumination cues are propagated coherently even under occlusions such as a book or a mask covering parts of the face. Furthermore, in zoom-out scenarios where later frames reveal previously unseen regions, Light-X continues to produce reasonable and consistent relighting for these newly visible areas. The corresponding video results are provided in the supplementary video.

D.13 ROBUSTNESS TO DEPTH NOISE

Since Light-X relies on projected point-cloud views as soft geometric cues, inaccuracies in depth estimation may introduce biased geometry and affect performance. Nevertheless, the method does not require highly accurate depth and remains robust under moderate noise levels. We conducted a controlled experiment on 12 randomly selected scenes. Using DepthCrafter (Hu et al., 2024) as the default depth estimator, we injected Gaussian noise into the depth maps:

$$\tilde{D} = D + \epsilon \cdot D, \quad \epsilon \sim \mathcal{N}(0, \text{rate}),$$

where *rate* controls the perturbation strength. The performance under different noise levels is summarized in Table H. As shown in Fig. K, Light-X maintains coherent illumination and motion consistency even when depth maps are perturbed with moderate Gaussian noise. Light-X degrades gracefully as noise increases and consistently outperforms baseline methods. Corresponding qualitative video results are provided in the supplementary video.

D.14 CHOICE OF THE RELIGHTING REFERENCE FRAME

Light-X does not rely on using the first frame as the relighting reference. During training, the relit frame is randomly sampled, and during inference any frame may be selected. In the main text, we adopt the first frame purely for implementation convenience and reproducibility.

To assess robustness to the choice of reference frame, we evaluate four strategies (“first”, “middle”, “last”, “random”) on 200 videos. As shown in Table I, Light-X achieves similar performance across all strategies, showing that the method is robust to the selection of the relighting reference frame.

D.15 USING LIGHT-X FOR DATA GENERATION

We investigate whether Light-X can be used to generate higher quality relit videos to further improve the training data. To this end, we relight 2k samples from the training set using Light-X and fine-tune the original model with this additional data. As shown in Table J, the fine-tuned model shows only marginal improvements, suggesting that the original Light-Syn data already provides sufficiently strong supervision and that real in-the-wild videos remain the primary source of learning signals.

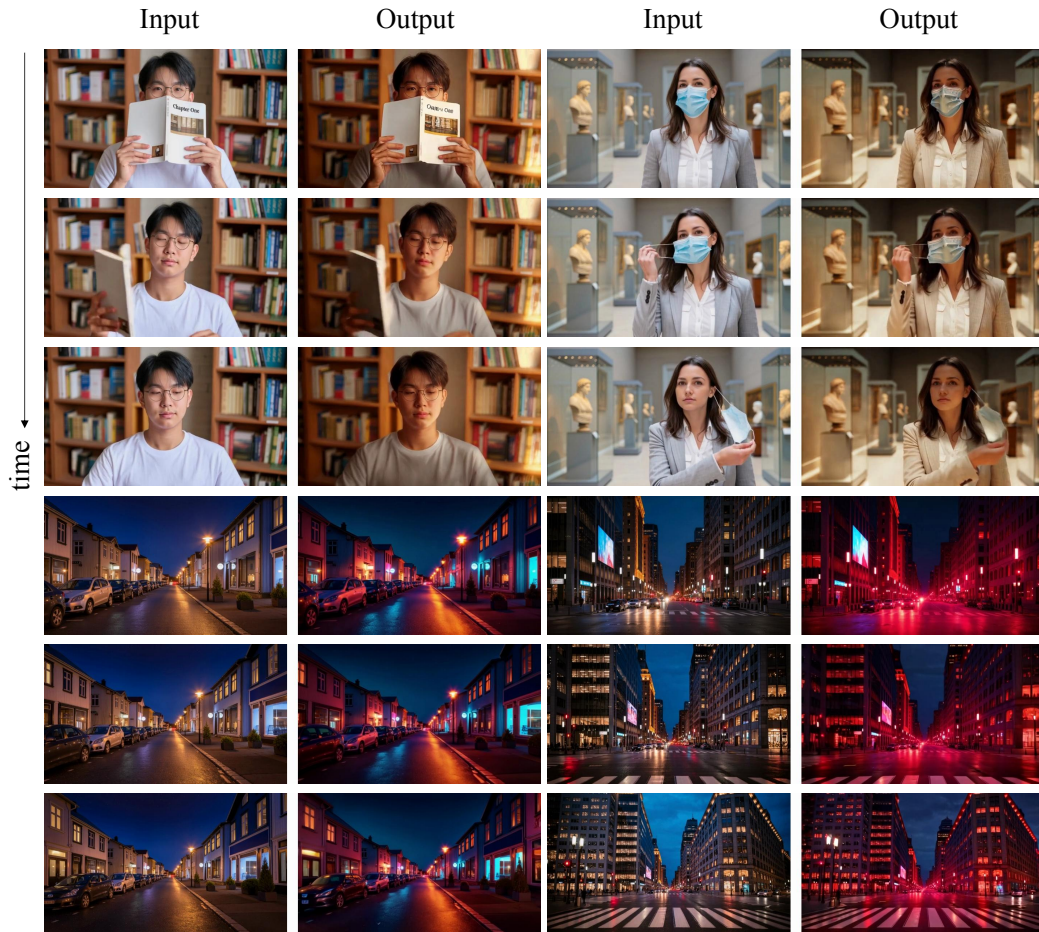


Figure I: Qualitative results showing robustness under occluded reference frames. Light-X maintains coherent illumination propagation even when the reference frame contains partial occlusions.

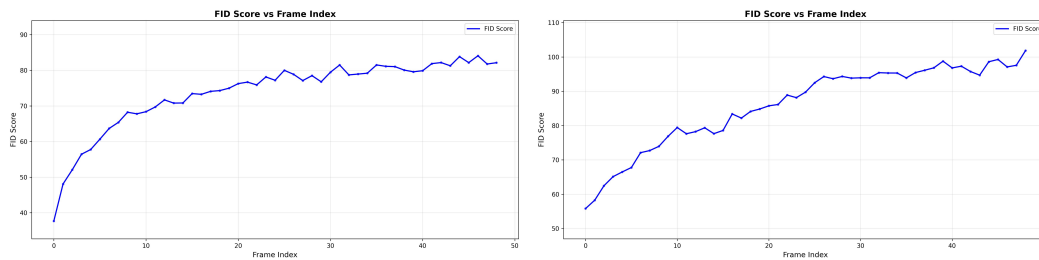


Figure J: FID variation as a function of temporal distance from the reference frame (the first frame). The left part corresponds to the video relighting setting, while the right part corresponds to the joint camera-illumination control setting.

Because synthetic relighting serves only as input rather than ground-truth supervision, its impact is naturally limited. However, the small but consistent gains indicate that generating a larger portion of the training data with Light-X, or exploring iterative self improvement strategies, could still offer potential benefits and represents an interesting direction for future work.

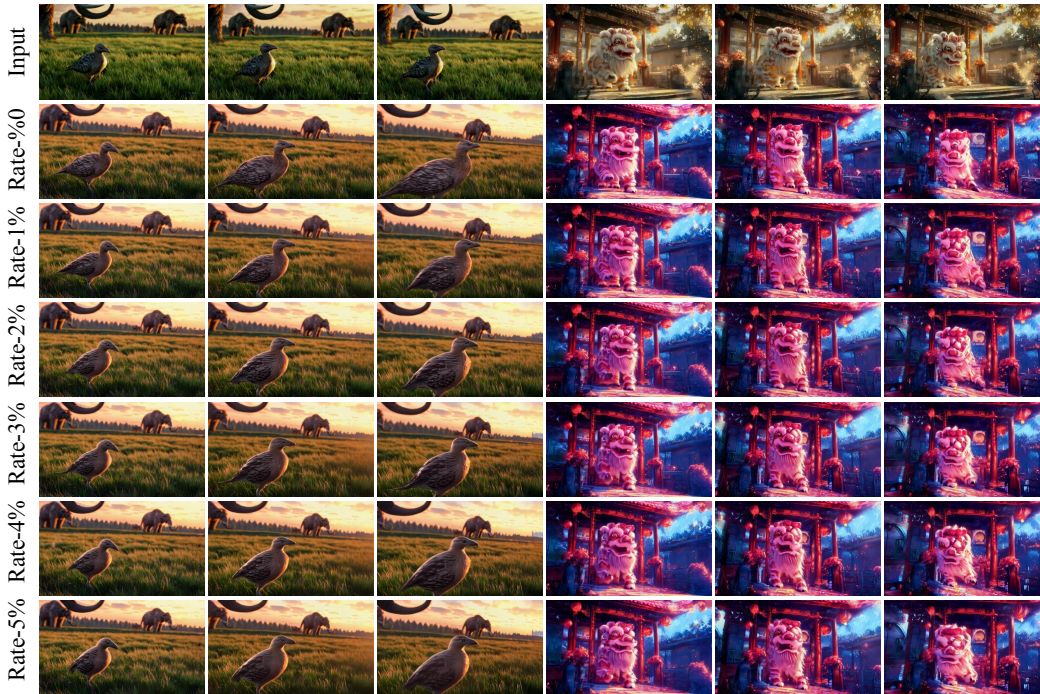


Figure K: Qualitative results under different depth noise levels. Light-X maintains coherent illumination and motion consistency even when depth maps are perturbed with moderate Gaussian noise.

Table H: Performance under increasing depth noise levels.

Method	FID ↓	Aesthetic ↑	Motion Pres. ↓	CLIP ↑
TC + IC-Light	/	0.556	14.199	0.977
TC + LAV	138.71	0.567	9.883	0.989
LAV + TC	155.09	0.581	13.768	0.989
TL-Free	127.77	0.585	9.533	0.990
Ours (rate = 0)	101.51	0.622	7.266	0.991
Ours (rate = 0.01)	107.01	0.619	9.632	0.989
Ours (rate = 0.02)	111.97	0.609	9.948	0.989
Ours (rate = 0.03)	111.44	0.607	10.672	0.989
Ours (rate = 0.04)	115.14	0.602	10.549	0.989
Ours (rate = 0.05)	116.67	0.602	10.350	0.988

D.16 USE OF SYNTHETIC RELIGHTING DATA

We do not adopt synthetic relighting data from graphics engines because such data often fails to capture the complexity and variability of real-world illumination. Our Light-Syn degradation pipeline instead uses in-the-wild videos as ground truth, providing lighting behavior that better matches the model’s training requirements. Moreover, IC-Light (Zhang et al., 2025b) already provides strong illumination priors from large-scale real and synthetic data, reducing the need for additional synthetic relighting.

To assess whether synthetic data can still bring benefits, we generated 2k synthetic samples with diverse viewpoints and lighting conditions using a DiffusionRenderer-style procedure (Liang et al., 2025). Representative examples are shown in Fig. L. These synthetic samples were mixed with Light-Syn data for training. As reported in Table K, incorporating synthetic relighting consistently degrades performance, suggesting that the domain gap between synthetic and real illumination distributions adversely affects learning. While synthetic relighting offers well-controlled illumination variations, more realistic and diverse synthetic pipelines are needed for it to become truly beneficial.

Table I: Performance under different choices of the relighting reference frame.

Strategy	FID ↓	Aesthetic ↑	Motion Pres. ↓	CLIP ↑
first	83.65	0.645	1.137	0.993
mid	84.85	0.634	1.249	0.993
last	89.78	0.639	1.133	0.993
random	85.97	0.639	1.277	0.993

Table J: Performance of models fine-tuned with Light-X generated data on the video relighting and joint camera-illumination control tasks.

Task	Method	FID ↓	Aesthetic ↑	Motion Pres. ↓	CLIP ↑
Video Relighting	Ours (original)	83.65	0.645	1.137	0.993
	Ours (fine-tuned)	82.00	0.643	1.134	0.993
Joint Cam-Illumination	Ours (original)	101.06	0.623	2.007	0.989
	Ours (fine-tuned)	99.35	0.622	2.171	0.989

E ADDITIONAL ABLATION ANALYSES

Beyond the quantitative ablations presented in Table 6 in the main text and the qualitative comparisons shown in Fig. D, we provide further analysis to better understand the roles of different components, with a focus on the training data composition and the global illumination control module.

E.1 TRAINING DATA

The three data sources in Light-Syn, including static, dynamic, and AI-generated data, contribute complementary information to the joint camera–illumination control task. Removing static data (a.i) weakens unseen-view synthesis, as static videos provide natural cross-view pairs for stabilizing geometry, as shown in Fig. N. Excluding dynamic data (a.ii) introduces motion artifacts and reduces temporal reliability, as illustrated in Fig. O. Omitting AI-generated data (a.iii) lowers robustness to rare lighting conditions, such as neon or scenes with very bright highlights, where brightness may decay; corresponding qualitative effects are shown in Fig. M. These observations align with the quantitative trends in Table 6 and further demonstrate that the full data mixture helps maintain fidelity, consistency, and stability under diverse lighting.

E.2 GLOBAL ILLUMINATION CONTROL MODULE

The global illumination control module is crucial for maintaining stable lighting behavior under complex illumination changes. Disabling this module (b.ii) leads to fading or abrupt shifts in brightness, particularly when the scene contains strong directional or spatially varying lighting. With the module enabled, the model is able to preserve coherent global lighting trends, preventing brightness drift and improving temporal consistency. The qualitative results are shown in Fig. P.

Table K: Performance comparison with and without synthetic relighting data on the video relighting and joint camera–illumination control tasks.

Task	Method	FID ↓	Aesthetic ↑	Motion Pres. ↓	CLIP ↑
Video Relighting	Ours (original)	83.65	0.645	1.137	0.993
	Ours (+ synthetic)	98.35	0.623	1.802	0.993
Joint Cam-Illumination	Ours (original)	101.06	0.623	2.007	0.989
	Ours (+ synthetic)	118.56	0.600	3.904	0.989

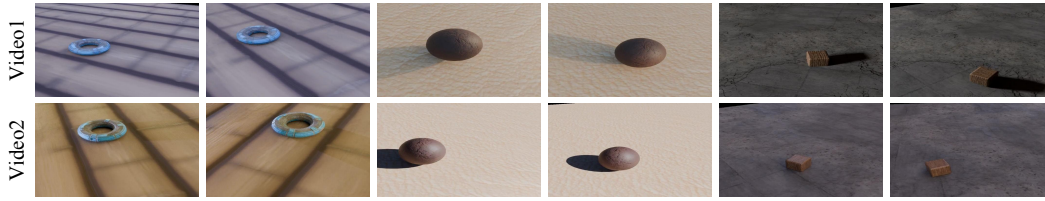


Figure L: Examples of synthetic relighting data generated using graphics engines. These samples exhibit controlled illumination and viewpoint variations.

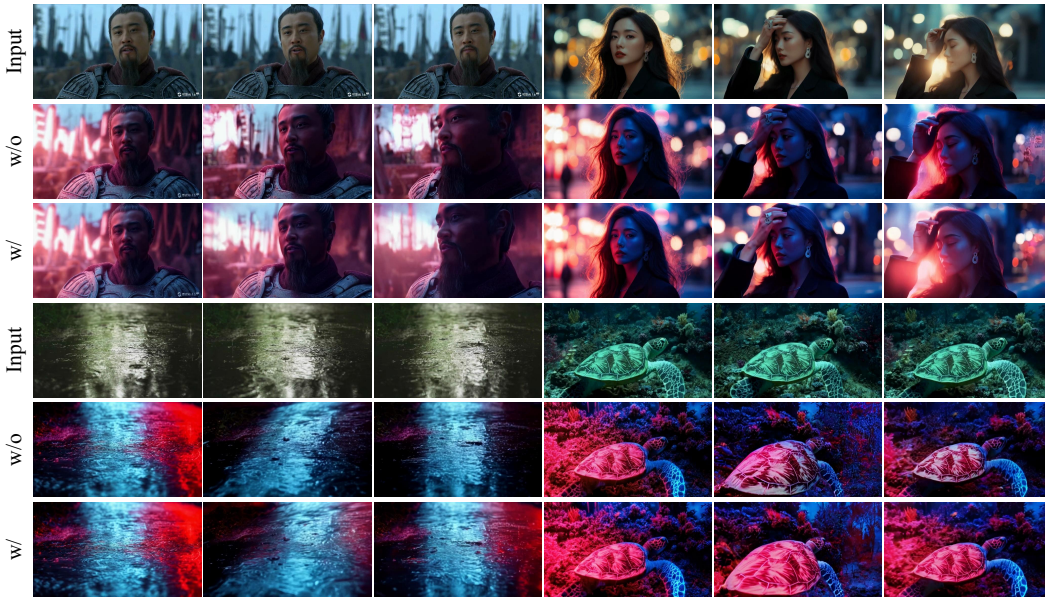


Figure M: Qualitative ablation of the **AI-generated data**.

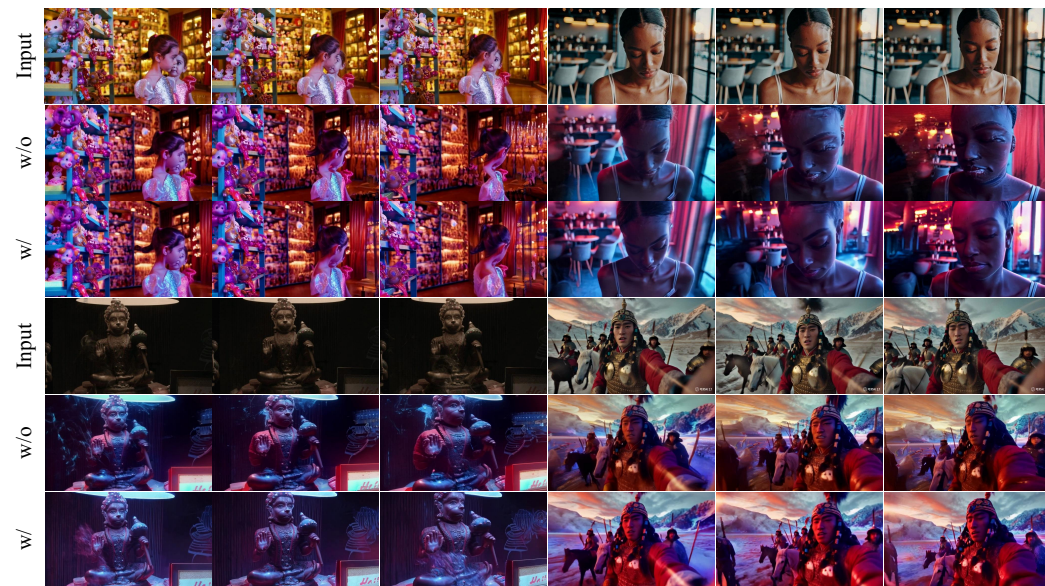


Figure N: Qualitative ablation of the **Static data**.

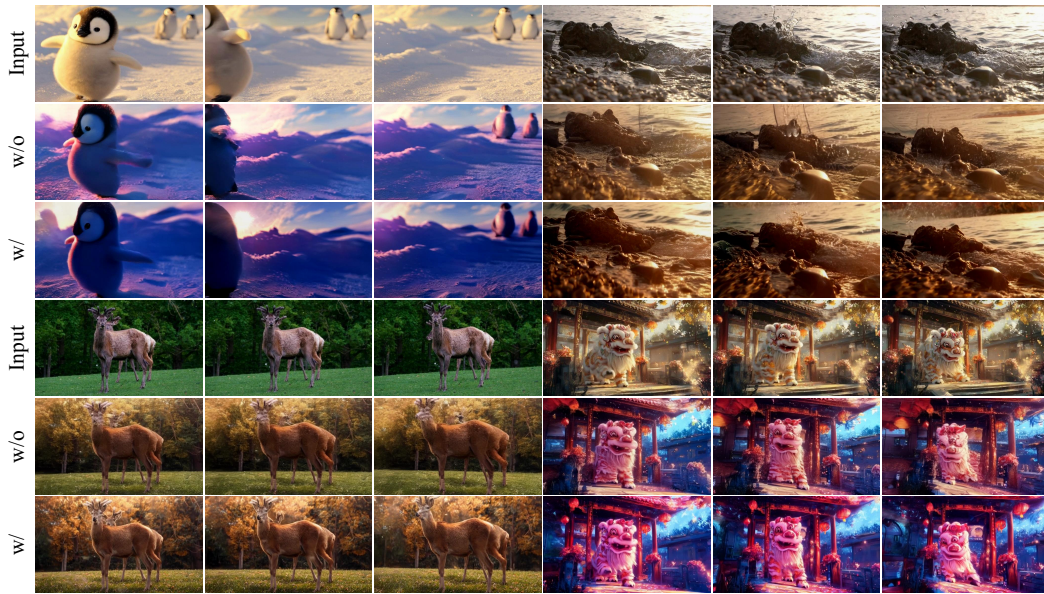


Figure O: Qualitative ablation of the **Dynamic data**.

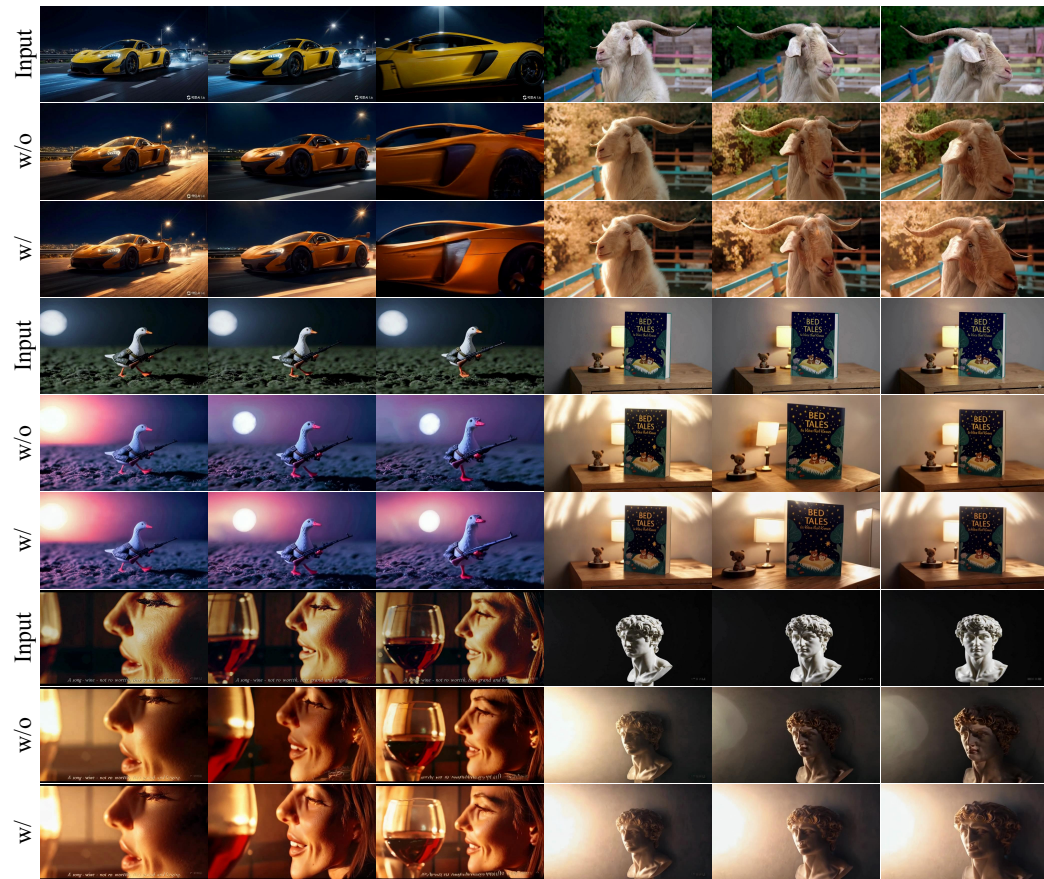


Figure P: Qualitative ablation of the **global illumination control**.

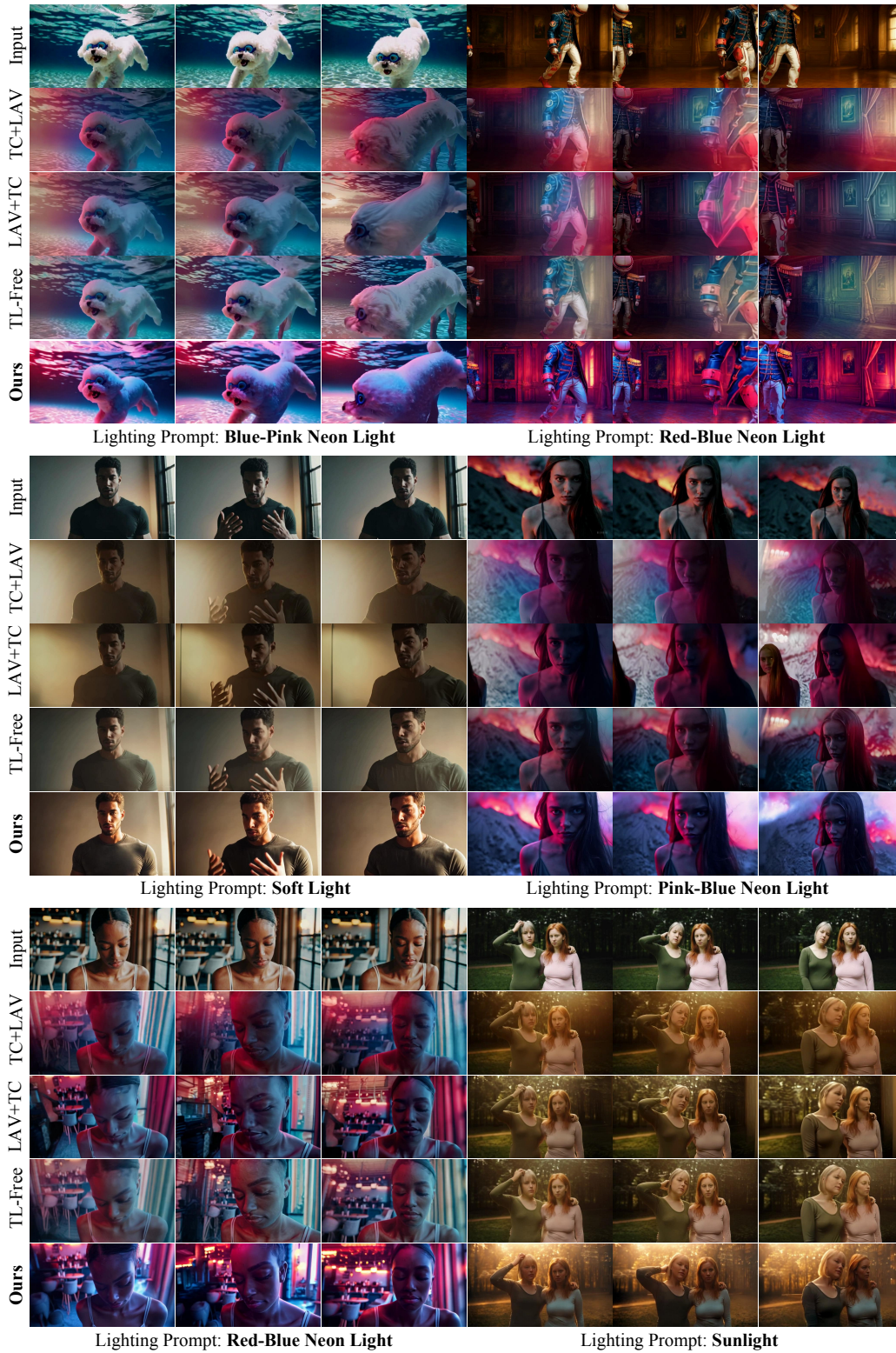


Figure Q: Qualitative comparison of joint camera-illumination control. Our method achieves superior relighting quality, temporal consistency, and realistic novel-view content generation compared to baseline methods.

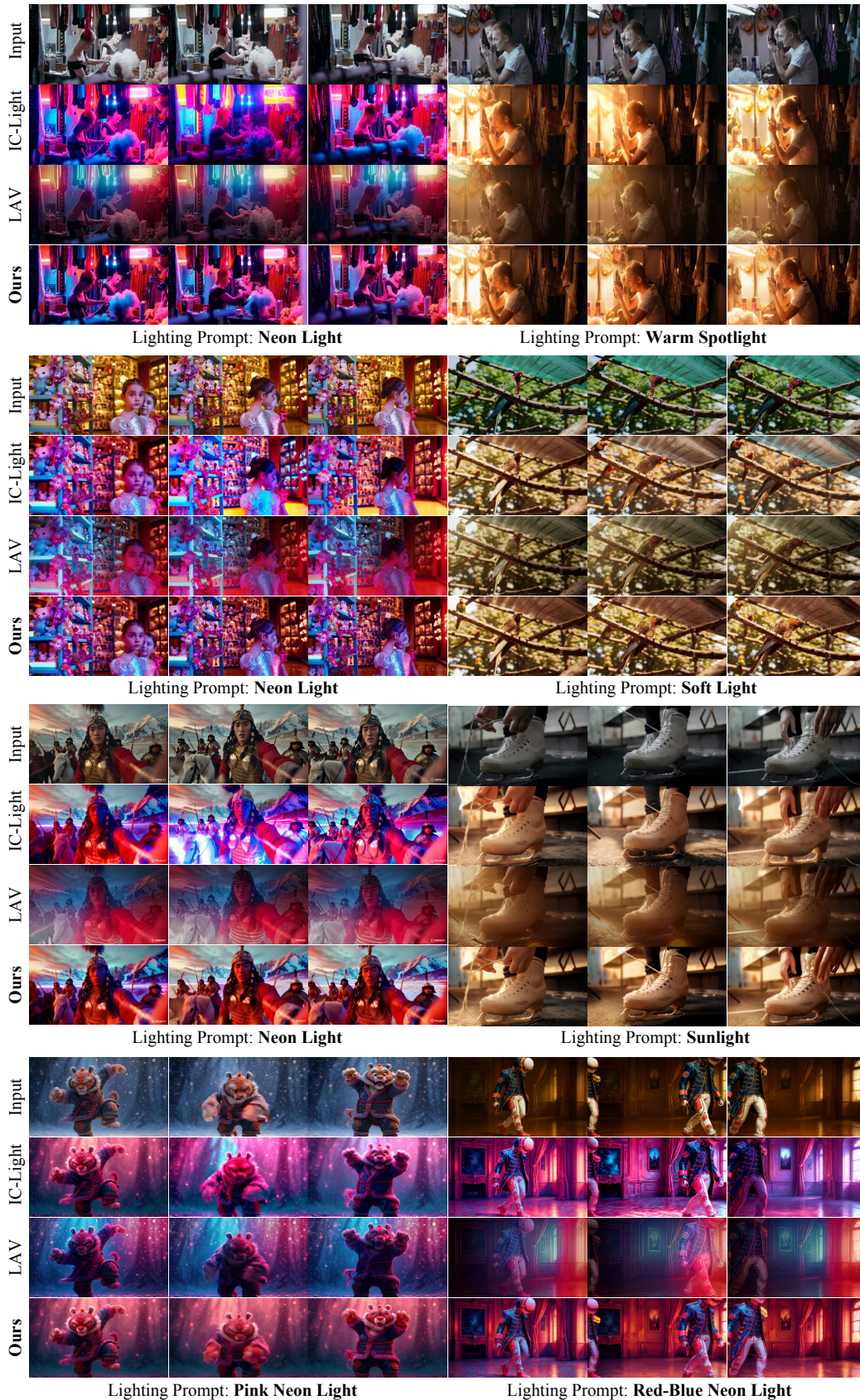


Figure R: Qualitative comparison of text-conditioned video relighting. Our method achieves superior both relighting quality and temporal consistency compared to baseline methods.



Figure S: Qualitative results of HDR map-conditioned video relighting. Given an input video and an HDR environment map, our model generates a relit video.

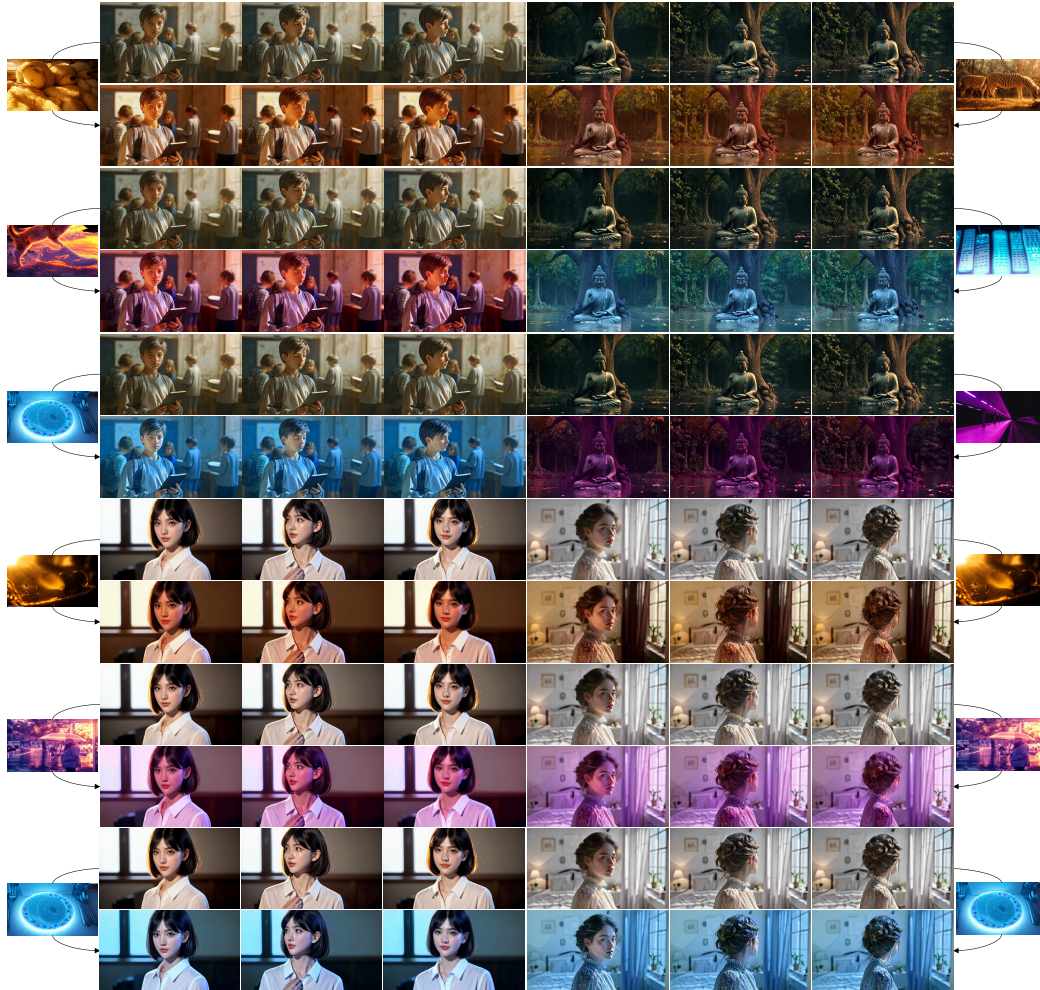


Figure T: Qualitative results of reference image-conditioned video relighting. Here, a reference image provides the target illumination style, which is transferred to the input video while preserving its content and motion.

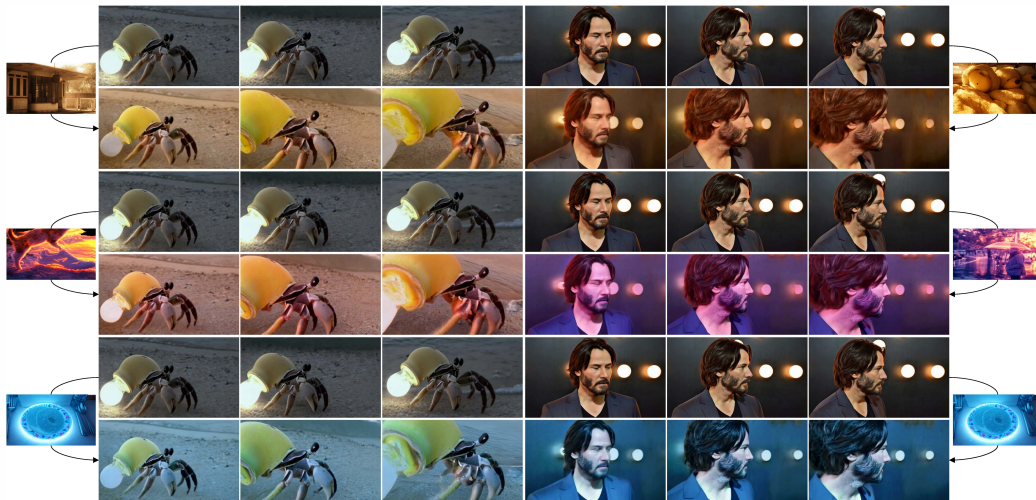


Figure U: Qualitative results of reference image-conditioned joint camera trajectory and illumination control. Here, a reference image provides the target illumination style, which is transferred to the input video while preserving its content and motion.